iScience

CellPress
OPEN ACCESS

Article

The proprotein convertase furin regulates the development of thymic epithelial cells to ensure central immune tolerance

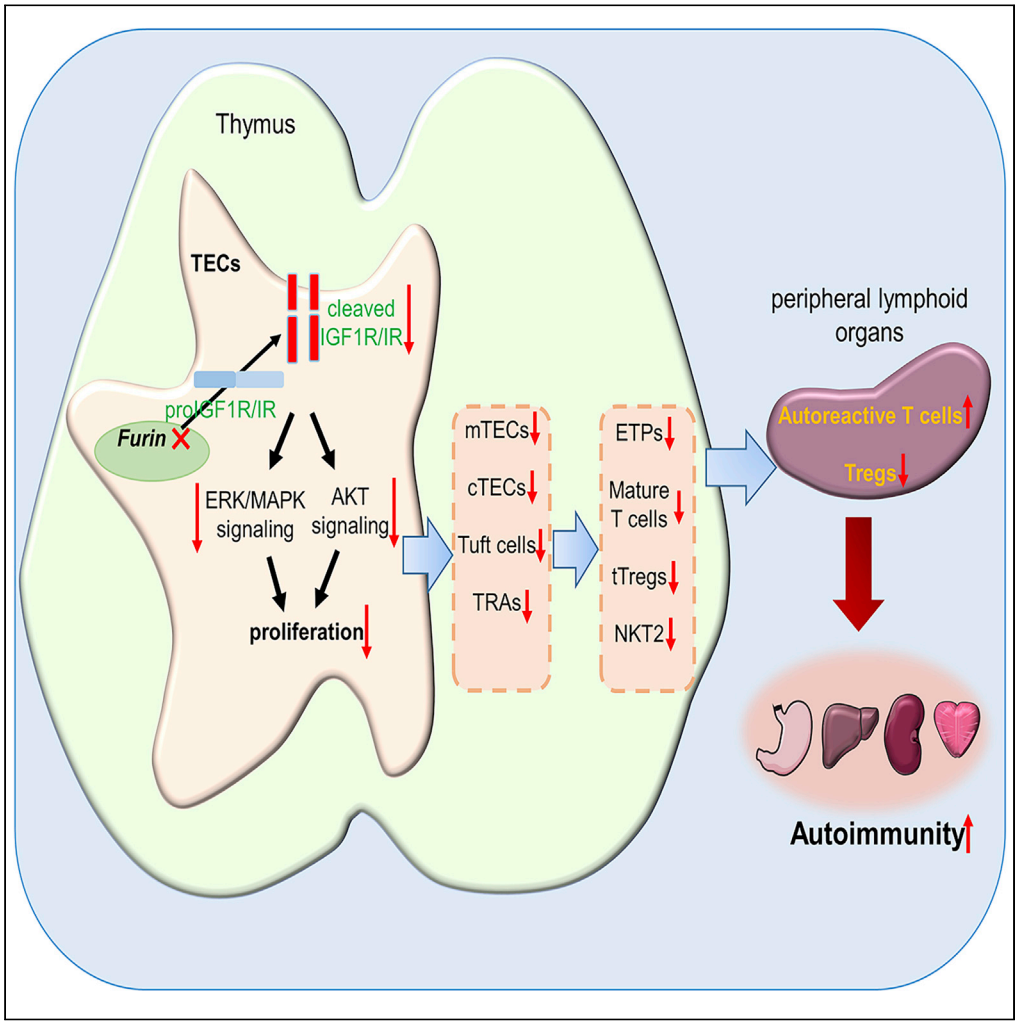

Zhanfeng Liang, Zhaoqi Zhang, Qian Zhang, ..., John W.M. Creemers, Baojun Zhang, Yong Zhao

bj.zhang@mail.xjtu.edu.cn (B.Z.)
zhaoy@ioz.ac.cn (Y.Z.)

Highlights

Furin is essential for the development of cTECs, mTECs, and thymic tuft cells

Furin regulates the proliferation of TECs via cleavage of proIGF1R and proIR

Furin expression in TECs is indispensable for multiple stages of thymopoiesis

TEC-expressed Furin is essential for the establishment of central immune tolerance

Liang et al., iScience 25, 105233
October 21, 2022
https://doi.org/10.1016/j.isci.2022.105233

iScience

CellPress
OPEN ACCESS

Article

The proprotein convertase furin regulates the development of thymic epithelial cells to ensure central immune tolerance

Zhanfeng Liang,[1,2,3,4,7] Zhaoqi Zhang,[1,2,7] Qian Zhang,[1,2,7] Xue Dong,[1,2] Xiaofeng Yang,[5] Jiayu Zhang,[1,2] Tong Lei,[1,2] John W.M. Creemers,[6] Baojun Zhang,[5,*] and Yong Zhao[1,2,3,4,8,*]

SUMMARY

The generation of mature T cells and establishment of central tolerance is predominantly orchestrated by thymic epithelial cells (TECs). Proprotein convertases are responsible for the proteolysis of proproteins into their mature bioactive counterparts. Here, we found that *Furin*, a member of the subtilisin/kexin-like PCs family, is highly expressed in TECs compared with other members of this family. TEC-specific deletion of *Furin* caused severe thymic atrophy and predominantly reduced the number of medullary TECs and thymic tuft cells, and to a less degree, cortical TECs. *Furin* deletion attenuated the proliferation of TECs, impaired thymopoiesis, and led to autoimmune disorders in mice. Furin promotes the development of TECs via cleavage of proIGF1 receptor and pro-Insulin receptor and the activation of downstream ERK/MAPK and Akt signaling pathways. Thus, this study uncovered the role of furin in TEC development and function and highlighted the importance of post-translational modification of immature proproteins in TEC biology.

INTRODUCTION

The development of functionally diverse and self-tolerant T cells in the thymus is critical for the continuous generation of adaptive immune responses. Thymic epithelial cells (TECs) elegantly orchestrate the generation of functionally competent T cells by providing niches for the attraction, proliferation, selection, and survival of developing T cells (Kadouri et al., 2019). TECs can be roughly categorized into cortical TECs (cTECs) and medullary TECs (mTECs) based on their anatomical structure and molecular characteristics (Barthlott et al., 2021). cTECs and mTECs are derived from the common progenitors expressing CD205 or β5t (Baik et al., 2013; Ohigashi et al., 2013), while the mTEC-restricted progenitors are identified as SSEA-1^{+}Cld3,4^{hi} TECs (Hamazaki et al., 2007; Sekai et al., 2014). The maturation of mTECs is defined by the concomitant upregulation of CD80, major histocompatibility complex class II (MHCII), autoimmune regulator (AIRE), and Fezf2 (Kadouri et al., 2019). Based on the expression of CD80 and MHCII, mTECs are subdivided into immature CD80^{lo}MHCII^{lo} mTEC^{lo} and mature CD80^{hi}MHCII^{hi} mTEC^{hi} subsets. The expression of AIRE and Fezf2 is critical for the expression of tissue-restricted antigens (TRAs) in mTECs (Liang et al., 2018; Sansom et al., 2014; Takaba et al., 2015). In contrast to the high heterogeneity of mTECs, the developmental heterogeneity of cTECs is not well defined. It has been known that the maturation of cTECs is defined by the acquisition of CD40 and the high expression of MHCII (Anderson and Takahama, 2012; Shakib et al., 2009). Recently, a new subset within terminally differentiated mTECs was identified; these cells are called thymic tuft cells because they share a large similarity with small-intestinal tuft cells (Bornstein et al., 2018; Miller et al., 2018). The differentiation of thymic tuft cells is predominantly regulated by transcription factor *Pou2f3* (Bornstein et al., 2018; Kadouri et al., 2019; Miller et al., 2018).

Proteolytic cleavage (PC) is one of the most important post-translational modifications of immature proproteins. The proteolytic cleavage of immature proproteins will generate functional mature proteins with critical roles in cell proliferation and survival, immunity and inflammation, and other important biological processes (Braun and Sauter, 2019). PCs are serine proteases that are responsible for the proteolytic cleavage of a variety of precursor proteins, including cytokines, extracellular matrix proteins, growth factors and their receptors, hormones, adhesion molecules, neuropeptides, and various proteins from pathogens (Brouwers et al., 2020; Seidah and Prat, 2012). *Furin*, also known as *Pcsk3*, was the first PC to be discovered

[1]State Key Laboratory of Membrane Biology, Institute of Zoology, Chinese Academy of Sciences, Beijing 100101, China

[2]University of Chinese Academy of Sciences, Beijing 100049 China

[3]Institute for Stem Cell and Regeneration, Chinese Academy of Sciences, Beijing 100101, China

[4]Beijing Institute for Stem Cell and Regenerative Medicine, Beijing 100101, China

[5]Department of Pathogenic Microbiology and Immunology, School of Basic Medical Sciences, Xi'an Jiaotong University, Xi'an, Shaanxi, China

[6]Laboratory of Biochemical Neuroendocrinology, Department of Human Genetics, KU Leuven, Leuven, Belgium

[7]These authors contributed equally

[8]Lead contact

*Correspondence: bj.zhang@mail.xjtu.edu.cn (B.Z.), zhaoy@ioz.ac.cn (Y.Z.)

https://doi.org/10.1016/j.isci.2022.105233

(Thomas, 2002). *Furin* and six other PC members (*Pcsk1*, *Pcsk2*, *Pcsk4*, *Pcsk5*, *Pcsk6*, and *Pcsk7*) constitute the subtilisin/kexin-like PCs family that cleave proproteins at paired basic amino acids with the motif R/K-X_n-R/K↓ (n = 0, 2, 4, or 6, and X is any aa, except Cys) (Al Rifai et al., 2017; He et al., 2020b; Susan-Resiga et al., 2011). Furin exhibits a strong preference for the cleavage of paired basic amino acids with the motif R-X-R/K-R↓ (Braun and Sauter, 2019; Jaaks and Bernasconi, 2017). The proprotein substrates of furin in mammals include growth factors and their receptors, hormones, and adhesion molecules (Braun and Sauter, 2019). Germline knockout of *Furin* is embryonically lethal (Roebroek et al., 1998), and furin is implicated in many biological processes, including ontogeny, tumor progression, cell-cell adhesion, pathogen infection, and inflammation (Bessonnard et al., 2015; Couture et al., 2015). Until now, the role of PCs in the development of TECs has been unknown. After finding that *Furin* is highly expressed in cTECs and mTECs compared to the other six members of the subtilisin/kexin-like PC family, we generated TEC-specific *Furin* ablation mice to study the role of furin in the development and differentiation of TECs. We showed here that TEC-specific ablation of *Furin* dramatically reduced the numbers of mTECs and, to a lesser degree, reduced the numbers of cTECs, which subsequently led to severe thymic atrophy. Moreover, TEC-specific ablation of *Furin* also substantially impaired the differentiation of thymic tuft cells. Importantly, TEC-specific ablation of *Furin* broke down the establishment of T cell central immune tolerance so that these mice displayed autoimmune disorders. Thus, our study elucidated a previously unrecognized role of proprotein convertase furin in TEC differentiation and the corresponding development of thymocytes in mice, supporting the importance of post-translational modification of proproteins, such as proteolytic cleavage, in regulating TEC development.

RESULTS

Furin deficiency remarkably impaired the development of thymic epithelial cells

To investigate the role of subtilisin/kexin-like PCs in TEC biology, we first assessed the expression of the seven subtilisin/kexin-like PCs in cTECs and mTECs according to the available RNA-seq data (Rodrigues et al., 2017). The results showed that the mRNA expression of *Furin* was much higher than the other six PC members in both cTECs and mTECs (Figure 1A). We thus focused our studies on the intrinsic role of *Furin* in TECs and generated mice with TEC-specific deletion of *Furin* by crossing mice with a loxP-flanked *Furin* allele to mice expressing the Cre recombinase under the control of the *Foxn1* promoter. The genotypes of homozygous ($Furin^{fl/fl}Foxn1^{Cre}$) and heterozygous ($Furin^{fl/+}Foxn1^{Cre}$) TEC-specific *Furin* deletion mice were shown in Figure S1A, and the mRNA and protein expression of *Furin* in TECs of wild-type (WT), $Furin^{fl/+}Foxn1^{Cre}$, and $Furin^{fl/fl}Foxn1^{Cre}$ mice were shown in Figures S1B and S1C.

We found that the heterozygous and homozygous knockout of *Furin* in TECs caused severe thymic atrophy and substantially reduced the ratio of thymus weight to body weight and the cellularity of thymocytes (Figures 1B–1D). Noticeably, the homozygous deletion of *Furin* in TECs caused obvious thymic atrophy and led to a significantly declined cell number of thymocytes and the ratio of thymus weight to body weight than heterozygous deletion of *Furin* in TECs did (Figures 1B–1D), indicating the potential dose-dependent role of *Furin* on the development of TECs in mice. The thymus is segregated anatomically into cortical and medullary regions that express its specific markers cytokeratin 8 (K8) and cytokeratin 5 (K5), respectively (Liang et al., 2021). Both H&E and immunofluorescence staining revealed that the thymic medulla of both $Furin^{fl/+}Foxn1^{Cre}$ and $Furin^{fl/fl}Foxn1^{Cre}$ mice dramatically declined compared with WT mice and that the cortical region of thymus in $Furin^{fl/fl}Foxn1^{Cre}$ mice also showed a decreased tendency (Figures 1E and 1F). Consistently, the frequency and absolute numbers of TECs in $Furin^{fl/+}Foxn1^{Cre}$ and $Furin^{fl/fl}Foxn1^{Cre}$ mice substantially decreased than $Furin^{fl/fl}$ control mice (Figures 1G and 1H). The percentage of mTECs was drastically reduced in $Furin^{fl/fl}Foxn1^{Cre}$ mice and moderately reduced in $Furin^{fl/+}Foxn1^{Cre}$ mice compared with WT mice (Figure 1I). The homozygous or heterozygous *Furin* ablation in TECs considerably reduced the absolute numbers of mTECs compared with WT mice (Figure 1J). In contrast, the frequency of cTECs was substantially elevated in $Furin^{fl/fl}Foxn1^{Cre}$ and $Furin^{fl/+}Foxn1^{Cre}$ mice compared with WT mice (Figure 1I), and homozygous or heterozygous *Furin* deletion only mildly diminished the numbers of cTECs (Figure 1J). These results indicated that furin regulated the development of mTECs likely in a dose-dependent manner and *Furin* deletion predominately impaired mTEC development and, to a lesser content, affected cTEC development.

We further examined the effect of *Furin* ablation on the development of TECs at the embryonic stage. The results showed that the total thymocyte number decreased significantly in $Furin^{fl/fl}Foxn1^{Cre}$ embryos compared with WT embryos (Figure S2A). The absolute cell number of TECs decreased obviously in

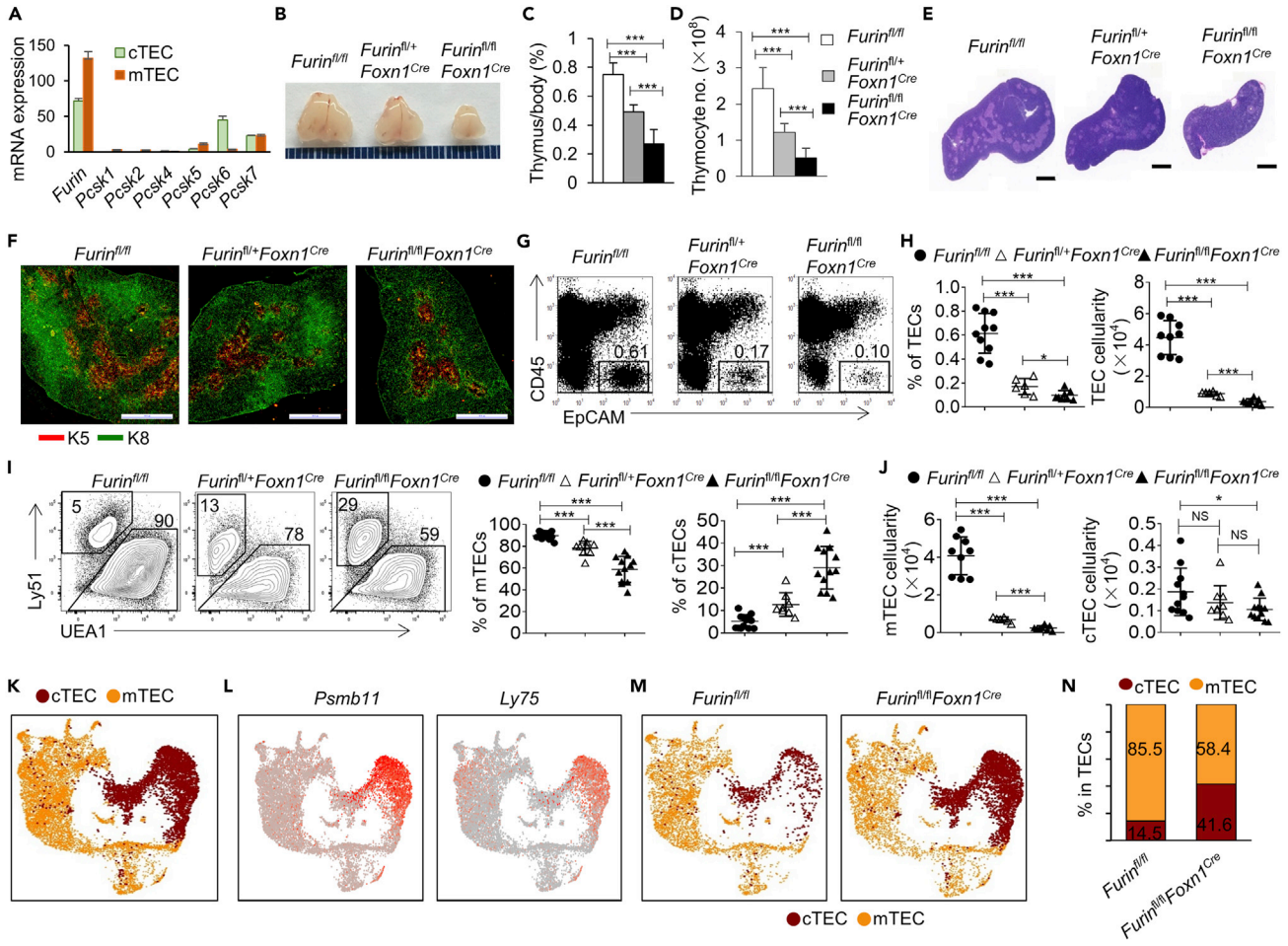

Figure 1. Homozygous or heterozygous deletion of *Furin* in TECs impaired the development of mTECs and cTECs

(A) The expression of subtilisin/kexin-like PCs (*Furin*, *Pcsk1*, *Pcsk2*, *Pcsk4*, *Pcsk5*, *Pcsk6*, and *Pcsk7*) in cTECs and mTECs. The transcripts per million (TPM) values of these genes are shown.

(B–D) The representative picture (B), the ratio of thymus weight to body weight (C), and average cellularity (D) of the thymus of 2-week-old WT, *Furin*$^{fl/+}$*Foxn1*^{Cre}, and *Furin*$^{fl/fl}$*Foxn1*^{Cre} mice (n = 6 to 12 per group).

(E) The representative H&E staining of thymus sections of 2-week-old WT, *Furin*$^{fl/+}$*Foxn1*^{Cre}, and *Furin*$^{fl/fl}$*Foxn1*^{Cre} mice. Scale bars: 1,000 μm.

(F) The staining of K5 (red) and K8 (green) for the frozen thymus sections derived from 2-week-old WT, *Furin*$^{fl/+}$*Foxn1*^{Cre}, and *Furin*$^{fl/fl}$*Foxn1*^{Cre} mice. Scale bars: 1,000 μm.

(G) Representative flow cytometry plots showing the frequency of CD45$^-$EpCAM$^+$ TECs in 2-week-old WT, *Furin*$^{fl/+}$*Foxn1*^{Cre}, and *Furin*$^{fl/fl}$*Foxn1*^{Cre} mice.

(H) Average frequency (left) and cellularity (right) of TECs from 2-week-old WT, *Furin*$^{fl/+}$*Foxn1*^{Cre}, and *Furin*$^{fl/fl}$*Foxn1*^{Cre} mice (n = 6 to 10 per group).

(I) Representative flow cytometry plots and average frequency of mTECs and cTECs in 2-week-old WT, *Furin*$^{fl/+}$*Foxn1*^{Cre}, and *Furin*$^{fl/fl}$*Foxn1*^{Cre} mice. mTECs were defined as CD45$^-$EpCAM$^+$UEA1$^+$Ly51$^-$, and cTECs were defined as CD45$^-$EpCAM$^+$UEA1$^-$Ly51$^+$.

(J) The cellularity of mTECs (left) and cTECs (right) of 2-week-old WT, *Furin*$^{fl/+}$*Foxn1*^{Cre}, and *Furin*$^{fl/fl}$*Foxn1*^{Cre} mice (n = 6 to 12 per group).

(K) UMAP visualization of 11,913 TECs of 2-week-old WT and *Furin*$^{fl/fl}$*Foxn1*^{Cre} mice, colored by cell types (cTECs and mTECs).

(L) UMAP visualization of the expression of cTEC marker genes (*Psmb11* and *Ly75*) used for cell cluster identification.

(M) UMAP visualization of WT TECs (4,301) and *Furin*-deficient TECs (4,086) from 2-week-old mice, colored by cell types (cTECs and mTECs).

(N) The proportions of cTECs and mTECs in 2-week-old WT and *Furin*$^{fl/fl}$*Foxn1*^{Cre} mice identified in (M).

Data are represented as mean ± SD *p < 0.05; ***p < 0.001; NS, not statistically different.

TEC-specific *Furin* knockout mice, although the frequency of TECs was comparable between WT and *Furin*$^{fl/fl}$*Foxn1*^{Cre} embryos (Figures S2B and S2C). Similar to postnatal stages, *Furin* ablation in TECs reduced the cell number of mTECs dramatically and the cell number of cTECs mildly (Figures S2D and S2E). We next examined the effect of *Furin* deletion on the development of TEC progenitors. CD205$^+$ TECs that could generate both cTECs and mTECs represent the common progenitors of cTECs and mTECs (Baik et al., 2013) and Cld3,4^{hi}SSEA-1$^+$ TECs were identified as mTEC progenitors (Sekai et al., 2014). We found that the proportions of both CD205$^+$ TECs and Cld3,4^{hi}SSEA-1$^+$ TECs were similar between WT and

Furin$^{fl/fl}$*Foxn1*^{Cre} embryos (Figures S2F and S2G), indicating *Furin* deletion did not alter the early development process of TECs. Combined with the results of 2-week-old mice, we concluded that *Furin* is indispensable for the development of TECs at the embryonic and postnatal stages.

To further assess the effect of *Furin* ablation on TEC development and heterogeneity, we detected the transcriptional profiles of TECs of 2-week-old WT and *Furin*$^{fl/fl}$*Foxn1*^{Cre} mice using single-cell RNA-seq (scRNA-seq) assays. Employing an unsupervised graph-based clustering strategy, 20 clusters of TECs and 5 clusters of non-TEC contaminants (clusters 8, 14, 19, 22, and 23) were identified (Figures S3A and S3B). Clusters 14 and 19, expressing CD4, CD8, and cTEC marker *Psmb11*, may represent thymic nurse cells, which envelop many viable thymocytes within their intracellular vesicles (Figure S3B). Clusters 8, 22, and 23 represent thymocytes, endothelial cells, and fibroblast contaminants, respectively (Figure S3B). Contaminated clusters were removed before further analysis, and all populations used were displayed in the Uni-form Mani-fold Approximation and Projection (UMAP) plots (Figure S4A). The cTECs and mTECs are obviously separated based on the cTEC-specific marker genes *Psmb11* and *Ly75* (Figures 1K and 1L), and the expressions of mTEC-specific genes (*AIRE*, *Fezf2*, *Ccl21a*, and *Cldn4*) were confirmed to be restricted to the mTEC population in the UMAP plots (Figure S4B). The top 10 representative genes in cTECs and mTECs are shown in Figure S4C. Consistent with the results obtained by flow cytometry (Figure 1I), the proportion of mTECs significantly decreased, and the proportion of cTECs significantly increased in *Furin*$^{fl/fl}$*Foxn1*^{Cre} mice compared with WT mice (Figures 1M and 1N). Collectively, *Furin* ablation in TECs significantly altered the proportion of mTECs and cTECs, drastically reduced the cell number of mTECs, and mildly diminished the cell number of cTECs.

Furin ablation had no obvious effect on the expression of maturation markers in thymic epithelial cells

We further examined the maturation process of mTECs and cTECs in mutant mice. The proportion of mature mTEC^{hi} (CD80^{+}MHCII^{hi}) subpopulations was overtly normal in *Furin*$^{fl/+}$*Foxn1*^{Cre} and *Furin*$^{fl/fl}$*Foxn1*^{Cre} mice compared with WT mice (Figure 2A). Similar results were observed for the mature AIRE^{+} mTEC populations (Figure 2B). However, the number of cells of these mature mTEC subsets were dramatically reduced as a result of the reduction in total mTEC number (Figures S5A and S5B). Similarly, the percentage of CD40^{+} cTECs was also unaltered by homozygous or heterozygous deletion of *Furin* (Figure 2C), but the cell numbers of CD40^{+} cTECs were obviously decreased (Figure S5C).

mTECs are highly heterogeneous and were recently defined into four major populations by scRNA-seq analysis (Bornstein et al., 2018). Thus, we further analyzed the effect of *Furin* ablation on the differentiation and maturation of mTECs at the scRNA-seq level. We performed cluster analyses based on the expression of the specific marker genes of four major mTEC subsets (Bornstein et al., 2018; Cowan et al., 2019). The representative genes of each cluster are shown in Figures 2D and S6A. The scRNA-seq analysis showed that the proportions of mTEC I, II, and III were overtly unaltered between WT and *Furin*$^{fl/fl}$*Foxn1*^{Cre} mice (Figures 2E and 2F) and the expression levels of marker genes for mTEC I, II, and III were similar between WT and *Furin*-deficient mTECs (Figure S6B), whereas the percentage of mTEC IV, a terminally differentiated mTEC subset called thymic tuft cells (Bornstein et al., 2018), was significantly reduced (about 2.5-fold) in *Furin*$^{fl/fl}$*Foxn1*^{Cre} mice compared to WT mice (Figures 2E and 2F).

Furin deletion resulted in a severe defect of thymic tuft cell differentiation

Thymic tuft cells are similar to mucosal tuft cells and express the canonical taste transduction pathway genes and IL-25 (Bornstein et al., 2018; Miller et al., 2018). We further examined the expression level of some representative genes (*Pou2f3*, *Gnat3*, *IL25,* and *L1cam*) of thymic tuft cells, and the results showed that the expression level of *Pou2f3*, *IL25,* and *L1cam* had no obvious change in *Furin*-deficient thymic tuft cells compared with WT thymic tuft cells, and only *Gnat3* exhibited reduced expression in thymic tuft cells after *Furin* ablation (Figures 3A and 3B), indicating *Furin* ablation mainly reduced the proportion of thymic tuft cells with little effect on the expression level of the representative genes of thymic tuft cells. Owing to the reduction in the proportion of thymic tuft cells, the results of bulk RNA-seq revealed that the expression of many genes that are highly expressed in thymic tuft cells (Table S1) (Bornstein et al., 2018) markedly decreased in mTECs obtained from *Furin*$^{fl/+}$*Foxn1*^{Cre} and *Furin*$^{fl/fl}$*Foxn1*^{Cre} mice compared with those from WT mice (Figure 3C). Consistently, there was significant negative enrichment of genes in the taste transduction pathway (Kyoto Encyclopedia of Genes and Genomes [KEGG]: mmu04742) in *Furin*$^{fl/+}$*Foxn1*^{Cre} and *Furin*$^{fl/fl}$*Foxn1*^{Cre} mTECs compared with WT mTECs (Figure 3D). These bioinformatic

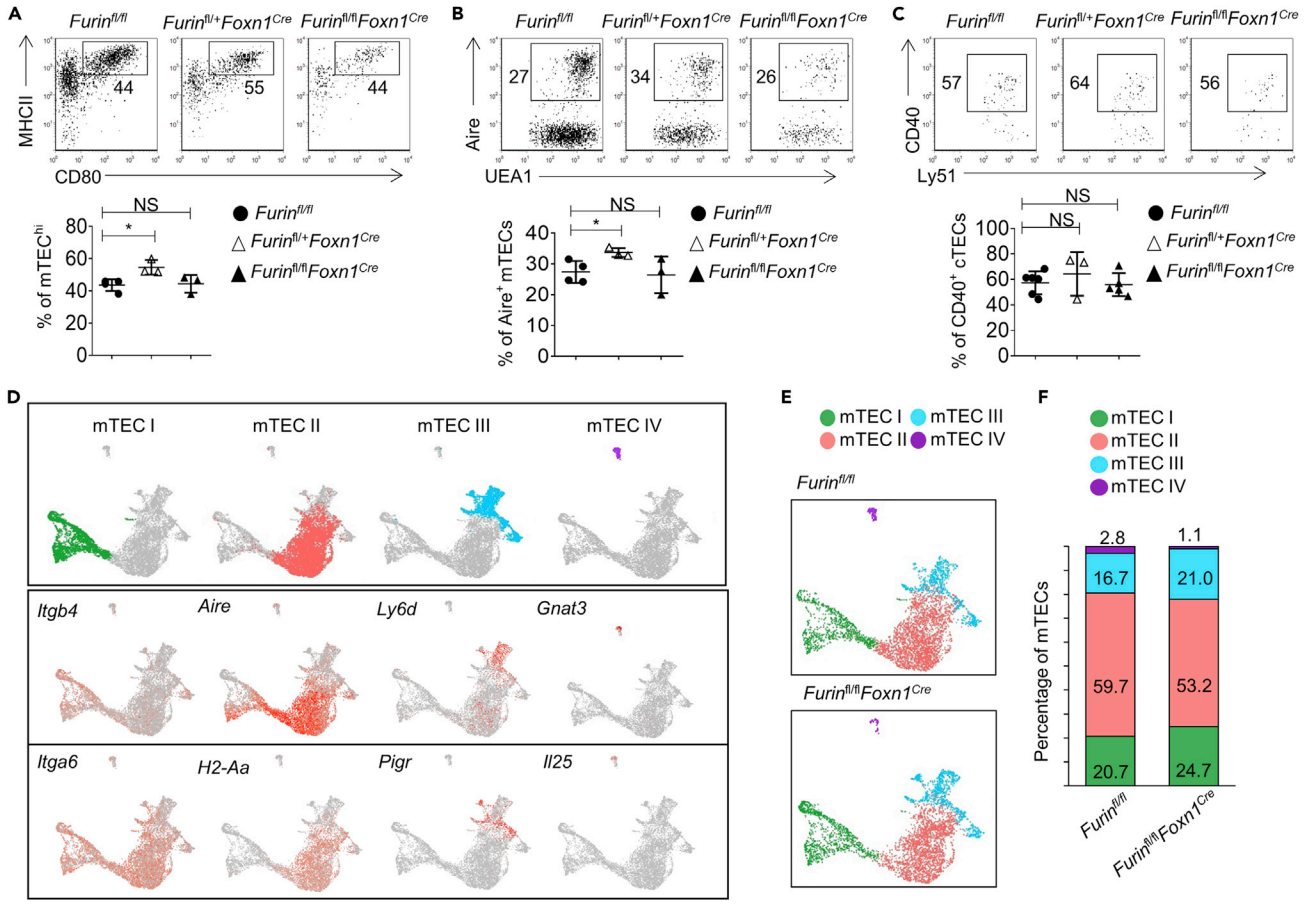

Figure 2. Homozygous or heterozygous deletion of *Furin* had no obvious effect on the expression of maturation markers in TECs

(A) The representative flow cytometry plots and frequency of mTEC^{hi} (CD80^{+}MHCII^{hi}) mTECs in 2-week-old WT, *Furin*$^{fl/+}$*Foxn1*^{Cre}, and *Furin*$^{fl/fl}$*Foxn1*^{Cre} mice.

(B) The representative flow cytometry plots and frequency of AIRE^{+} mTECs of 2-week-old WT, *Furin*$^{fl/+}$*Foxn1*^{Cre}, and *Furin*$^{fl/fl}$*Foxn1*^{Cre} mice.

(C) The representative flow cytometry plots and frequency of CD40^{+} cTECs in WT, *Furin*$^{fl/+}$*Foxn1*^{Cre}, and *Furin*$^{fl/fl}$*Foxn1*^{Cre} mice. In panels A-C, at least three mice were analyzed for each genotype.

(D) UMAP visualization of four individual mTEC subsets (above) clustered based on transcriptional similarity and the expression of known marker genes used for cell cluster identification.

(E) UMAP visualization of mTECs in WT and *Furin*$^{fl/fl}$*Foxn1*^{Cre} mice, colored by cell types.

(F) The proportion of mTEC I, II, III, and IV in WT and *Furin*$^{fl/fl}$*Foxn1*^{Cre} mice identified in (E).

Data are represented as mean ± SD *p < 0.05; NS, not statistically different.

information prompted us to further investigate the role of *Furin* in the differentiation of thymic tuft cells. It has been shown that thymic tuft cells exhibit high DCLK1 expression (Bornstein et al., 2018; Miller et al., 2018). Flow cytometry analysis showed that both the frequency and cell number of thymic tuft cells significantly decreased in *Furin*$^{fl/+}$*Foxn1*^{Cre} and *Furin*$^{fl/fl}$*Foxn1*^{Cre} mice compared with WT mice (Figures 3E and 3F). Consistently, the reduction of DCLK1^{+} thymic tuft cells was confirmed by immunofluorescence staining of thymic sections (Figure 3G). To further examine whether *Furin* deletion favorably impaired the differentiation of thymic tuft cells, we subdivided mTECs into TAC-TEC, *Ccl21a*-high, *Aire*-positive, Late-*Aire*, and Tuft subsets according to another recent publication (Wells et al., 2020). The results showed that the proportion of Tuft subsets reduced obviously and the proportion of the other subsets had no detectable change in *Furin*$^{fl/fl}$*Foxn1*^{Cre} mice compared with WT mice (Figures S6C and S6D). Collectively, these results indicated that TEC-specific deletion of *Furin* severely impaired the differentiation of thymic tuft cells.

Furin deletion decreased cell proliferation of thymic epithelial cells

Next, we explored the molecular mechanisms that caused the reduction of mTECs and cTECs in *Furin*$^{fl/+}$-*Foxn1*^{Cre} and *Furin*$^{fl/fl}$*Foxn1*^{Cre} mice. We examined the altered biological processes in mTECs and cTECs of

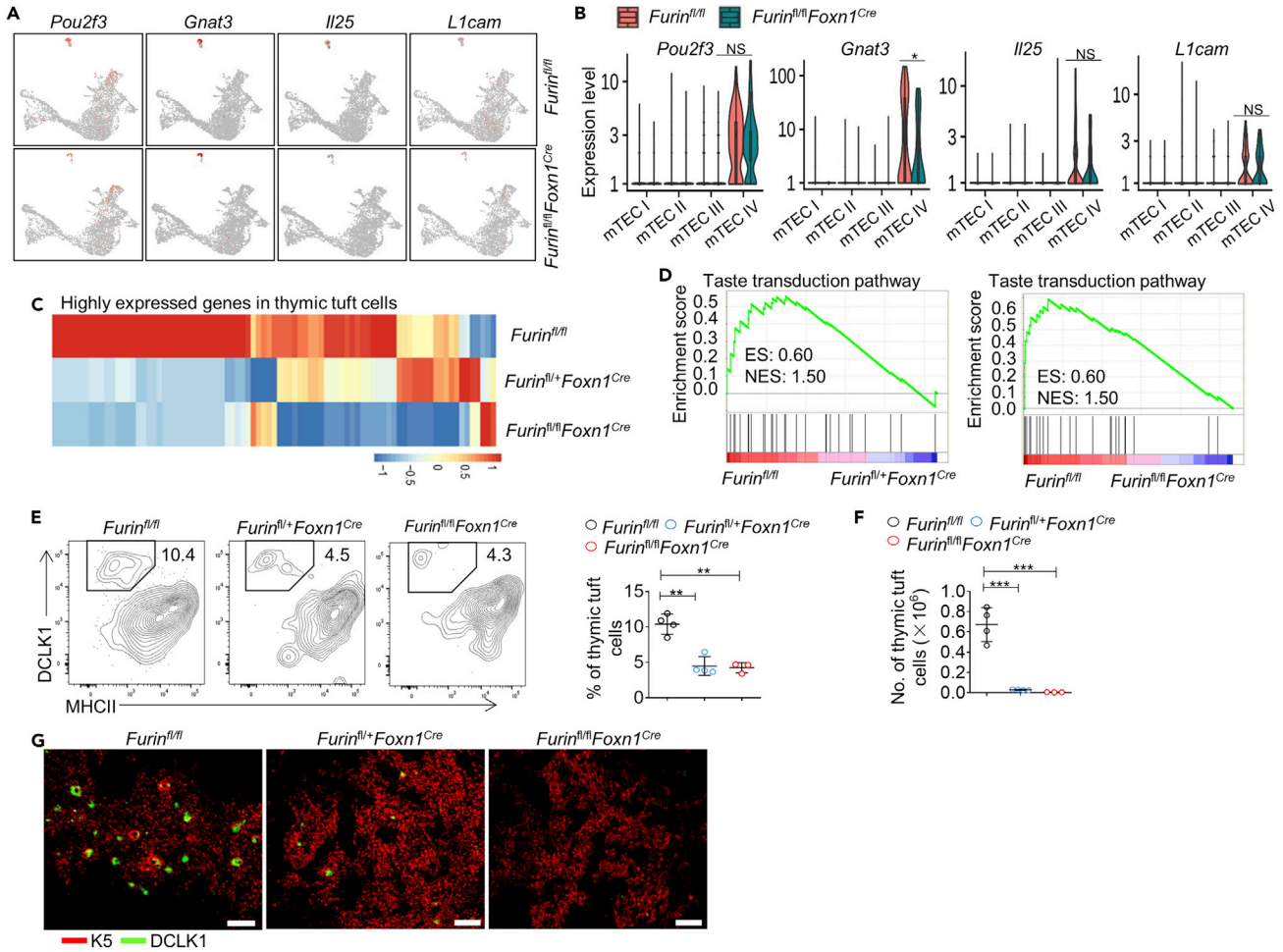

Figure 3. The differentiation of thymic tuft cells was severely impaired in *Furin*$^{fl/+}$*Foxn1*^{Cre} and *Furin*$^{fl/fl}$*Foxn1*^{Cre} mice

(A) UMAP plots showing the expression of representative thymic tuft cell marker genes in mTECs of 2-week-old WT and *Furin*$^{fl/fl}$*Foxn1*^{Cre} mice.

(B) Violin plots showing the expression of representative thymic tuft cell marker genes in mTEC I, II, III, and IV according to the scRNA-seq data.

(C) Heatmap showing the expression of genes that are highly expressed in thymic tuft cells in mTECs of 2-week-old WT, *Furin*$^{fl/+}$*Foxn1*^{Cre}, and *Furin*$^{fl/fl}$*Foxn1*^{Cre} mice according to the bulk RNA-seq data.

(D) Gene Set Enrichment Analysis (GSEA) was performed with the genes of the taste transduction pathway (KEGG: mmu04742) in mTECs of WT, *Furin*$^{fl/+}$*Foxn1*^{Cre}, and *Furin*$^{fl/fl}$*Foxn1*^{Cre} mice according to the bulk RNA-seq data.

(E) The representative flow cytometry plots (left) and percentage (right) of thymic tuft cells in 2-week-old WT (n = 4), *Furin*$^{fl/+}$*Foxn1*^{Cre} (n = 4), and *Furin*$^{fl/fl}$*Foxn1*^{Cre} (n = 3) mice.

(F) The number of thymic tuft cells in 2-week-old WT (n = 4), *Furin*$^{fl/+}$*Foxn1*^{Cre} (n = 4), and *Furin*$^{fl/fl}$*Foxn1*^{Cre} (n = 3) mice.

(G) Immunofluorescence staining of DCLK1 (green) and K5 (red) of the thymic section of 2-week-old WT, *Furin*$^{fl/+}$*Foxn1*^{Cre}, and *Furin*$^{fl/fl}$*Foxn1*^{Cre} mice. Scale bars: 1,000 μm.

Data are represented as mean ± SD *p < 0.05; **p < 0.01; ***p < 0.001; NS, not statistically different.

Furin$^{fl/+}$*Foxn1*^{Cre} and *Furin*$^{fl/fl}$*Foxn1*^{Cre} mice compared to WT mice, using gene set variation analysis (GSVA). The RNA-seq count matrix (Table S2) was used for this analysis, and the results were listed in Table S3. The results revealed that there was no obvious expression change in the genes of the apoptosis pathway in mTECs and cTECs of *Furin*$^{fl/+}$*Foxn1*^{Cre} and *Furin*$^{fl/fl}$*Foxn1*^{Cre} mice compared with WT mice (Figure 4A). Consistent with the bioinformatic information, the apoptosis of mTECs and cTECs of *Furin*$^{fl/+}$*Foxn1*^{Cre} and *Furin*$^{fl/fl}$*Foxn1*^{Cre} mice was similar to that in the littermate controls as shown by cleaved caspase3 staining (Figures 4B and 4C). In contrast, the genes in cell proliferation-related biological processes gradually decreased in mTECs and cTECs of *Furin*$^{fl/+}$*Foxn1*^{Cre} and *Furin*$^{fl/fl}$*Foxn1*^{Cre} mice (Figure 4A). Importantly, the frequency of Ki67^{+} proliferating mTECs and cTECs dramatically decreased in *Furin*$^{fl/fl}$*Foxn1*^{Cre} mice and decreased more moderately in *Furin*$^{fl/+}$*Foxn1*^{Cre} mice compared with WT mice as detected by flow cytometry (Figures 4D and 4E). Similarly, the incorporation of bromodeoxyuridine (BrdU)

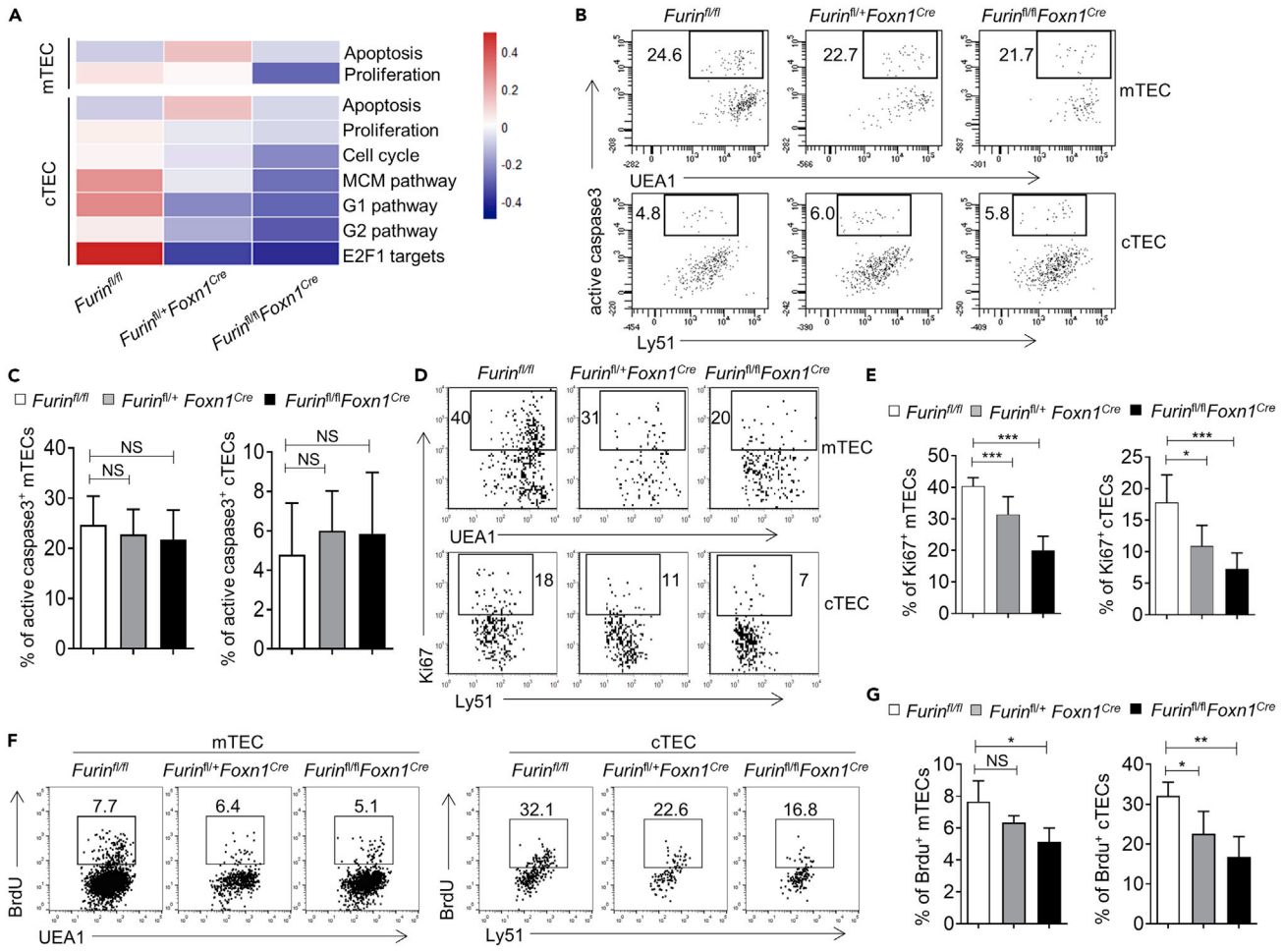

Figure 4. The proliferation of mTECs and cTECs decreased in *Furin*$^{fl/+}$*Foxn1*^{Cre} and *Furin*$^{fl/fl}$*Foxn1*^{Cre} mice

(A) A row-normalized heatmap showing the expression of gene pathways involved in apoptosis and proliferation in mTECs and cTECs of 2-week-old WT, *Furin*$^{fl/+}$*Foxn1*^{Cre}, and *Furin*$^{fl/fl}$*Foxn1*^{Cre} mice.

(B) Representative flow cytometry plots showing the expression of active caspase3 on mTECs and cTECs of newborn WT, *Furin*$^{fl/+}$*Foxn1*^{Cre}, and *Furin*$^{fl/fl}$*Foxn1*^{Cre} mice.

(C) Statistical analysis of active caspase3^{+} mTECs and cTECs of newborn WT, *Furin*$^{fl/+}$*Foxn1*^{Cre}, and *Furin*$^{fl/fl}$*Foxn1*^{Cre} mice. At least four mice were analyzed for each genotype.

(D) Representative flow cytometry plots showing the expression of Ki67 on mTECs and cTECs of newborn WT, *Furin*$^{fl/+}$*Foxn1*^{Cre}, and *Furin*$^{fl/fl}$*Foxn1*^{Cre} mice.

(E) Statistical analysis of Ki67^{+} mTECs and cTECs of newborn WT (n = 11), *Furin*$^{fl/+}$*Foxn1*^{Cre} (n = 4), and *Furin*$^{fl/fl}$*Foxn1*^{Cre} (n = 4) mice.

(F and G) The representative flow cytometry plots (F) and frequency (G) of BrdU^{+} mTECs and cTECs of 2-week-old WT, *Furin*$^{fl/+}$*Foxn1*^{Cre}, and *Furin*$^{fl/fl}$*Foxn1*^{Cre} mice. At least three mice were analyzed for each genotype.

Data are represented as mean ± SD *p < 0.05; **p < 0.01; ***p < 0.001; NS, not statistically different.

in mTECs and cTECs of *Furin*$^{fl/+}$*Foxn1*^{Cre} and *Furin*$^{fl/fl}$*Foxn1*^{Cre} mice was also decreased compared with WT mice as measured 24 h after single pulse BrdU labeling *in vivo* (Figures 4F and 4G). Recently, Wells et al. showed that the highly proliferative mTECs are mainly restricted to TAC-TEC subset (Wells et al., 2020) and we further analyzed the expression of some representative proliferation-related genes in different TEC subsets according to this publication. The scRNA-seq results showed that the expression of some representative proliferation-related genes, including *Ccnd1*, *Ccnd2*, *Cdk4*, and *Ranbp1*, showed high expression in TAC-TEC and *Ccl21a*-high mTEC subpopulations and the expression of these genes decreased significantly in TAC-TEC and *Ccl21a*-high TEC subsets of *Furin*$^{fl/fl}$*Foxn1*^{Cre} mice compared with that of WT mice (Figure S7A). We further examined the expression Ki67 in CD80^{+} and CD80^{-} mTEC subsets and we found that the expression of Ki67 decreased in both CD80^{+} and CD80^{-} mTEC subsets of *Furin*-deleted mice (Figures S7B and S7C). To further prove the pro-proliferation role of furin in TECs, *Furin* was overexpressed in mTEC cell line 1C6, and the proliferation of *Furin* overexpressed cells was

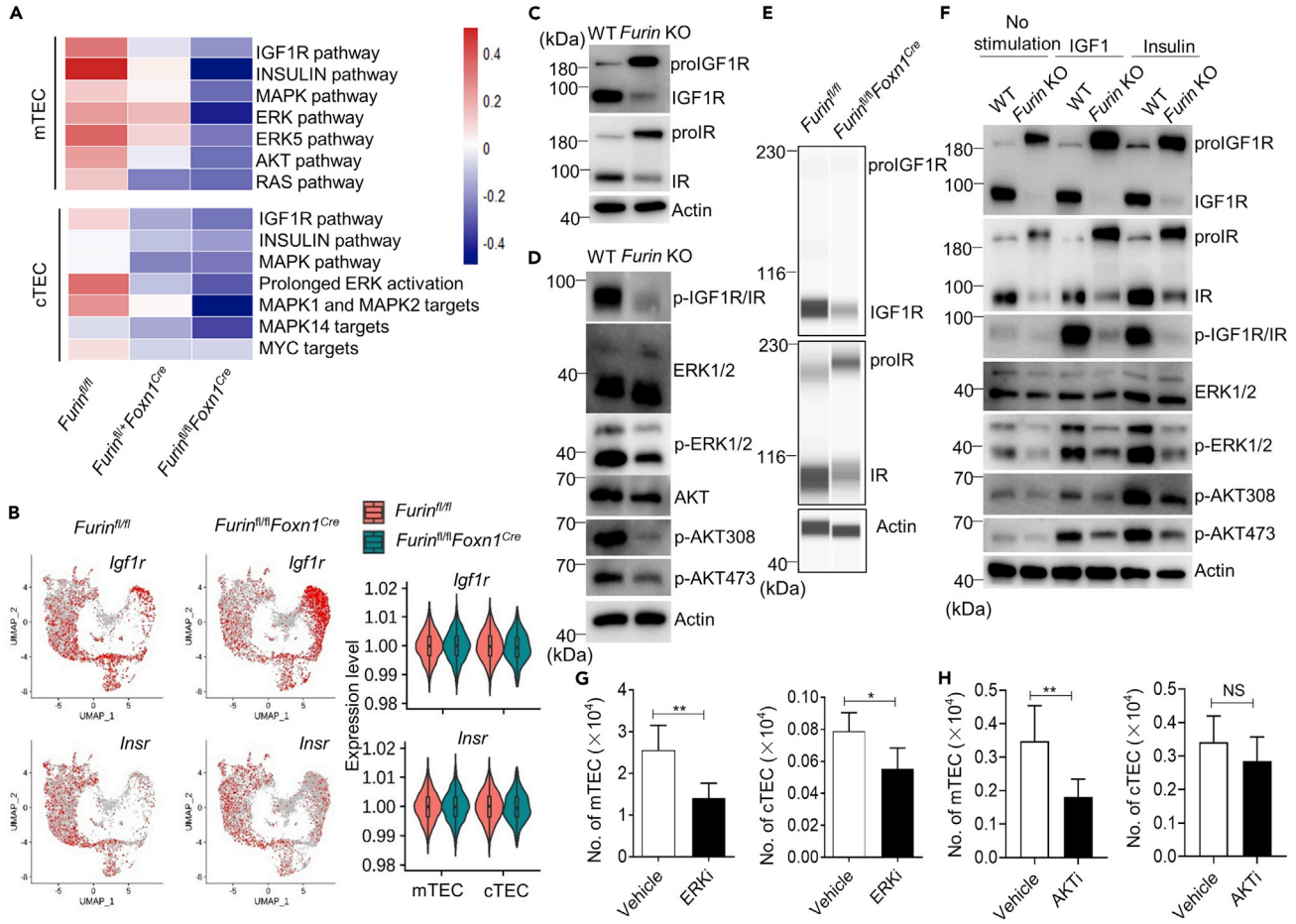

Figure 5. Furin promoted the development and proliferation of TECs via proteolytic cleavage of proIGF1R and proIR

(A) A row-normalized heatmap showing the expression of gene pathways that gradually decreased in mTECs and cTECs of 2-week-old WT, *Furin*$^{fl/+}$*Foxn1*^{Cre}, and *Furin*$^{fl/fl}$*Foxn1*^{Cre} mice.

(B) UMAP plots (left) and violin plots (right) showing the expression of *Igf1r* and *Insr* on mTECs and cTECs of 2-week-old WT and *Furin*$^{fl/fl}$*Foxn1*^{Cre} mice.

(C) Immunoblotting of cell lysates of cultured WT and *Furin* KO TECs for detecting the cleavage of proIGF1R and proIR.

(D) Immunoblotting of cell lysates of cultured WT and *Furin* KO TECs for detecting the phosphorylation of IGF1R/IR, ERK1/2, and Akt (Thr308 and Ser473).

(E) mTECs of WT and *Furin*$^{fl/fl}$*Foxn1*^{Cre} mice were sorted by flow cytometry, and cell lysates were analyzed by Simple Western to detect the cleavage of proIGF1R and proIR.

(F) Cultured WT and *Furin* KO TECs were starved overnight following stimulation with exogenous IGF1 (100 ng/mL) and insulin (200 ng/mL) for 20 min, and cell lysates were analyzed by immunoblot for detecting the phosphorylation of IGF1R/IR, ERK1/2, and Akt (Thr308 and Ser473). In panels C-F, the results are representative of three independent experiments.

(G) The numbers of mTECs and cTECs in ERK inhibitor (SCH772984) treated mice (n = 4) and control mice (n = 5).

(H) The numbers of mTECs and cTECs in Akt inhibitor (MK-2206) treated fetal thymic lobes (n = 6) and control fetal thymic lobes (n = 7).

Data are represented as mean ± SD *p < 0.05; **p < 0.01; NS, not statistically different.

detected. The results revealed that *Furin* overexpression significantly increased the proliferation of 1C6 cells as assessed by 5-Ethynyl-2′-deoxyuridine (EdU) incorporation (Figures S7D and S7E). In summary, these results demonstrated that furin is essential for the proliferation of TECs.

Furin regulated thymic epithelial cell development via cleavage of proIGF1R and proIR

We further examined the signaling pathways that account for the impaired development and proliferation of TECs in *Furin*$^{fl/+}$*Foxn1*^{Cre} and *Furin*$^{fl/fl}$*Foxn1*^{Cre} mice. GSVA analysis revealed that the IGF1R and insulin pathways and their downstream ERK/MAPK and Akt pathways gradually declined in mTECs and cTECs of *Furin*$^{fl/+}$*Foxn1*^{Cre} and *Furin*$^{fl/fl}$*Foxn1*^{Cre} mice (Figure 5A). It has been shown that IGF1 and insulin promoted thymus development and TEC proliferation (Binz et al., 1990; Chu et al., 2008; de Mello Coelho et al., 2002). Moreover, proIGF1R and proIR are well-established *Furin* proteolytic substrates (Khatib

et al., 2001; Roebroek et al., 2004). Thus, we postulated that the impaired development and proliferation TECs in *Furin*$^{fl/+}$*Foxn1*^{Cre} and *Furin*$^{fl/fl}$*Foxn1*^{Cre} mice may be caused by the proteolytic blockage of proIGF1R and proIR, which subsequently results in the attenuation of the ERK/MAPK and Akt pathways. The mRNA expression of *Igf1r* and *Insr* was comparable in mTECs and cTECs of WT and *Furin*$^{fl/fl}$*Foxn1*^{Cre} mice (Figure 5B), indicating that the downregulation of the IGF1R and insulin pathways was not a result of the transcriptional alteration of *Igf1r* and *Insr*. Because of the scarcity of the freshly isolated TECs, we investigated the cleavage of proIGF1R and proIR using a TEC *in vitro* culture system (Liang et al., 2018) by culturing TECs of ER-*Furin* mice in which *Furin* was deleted by treatment with tamoxifen. We found that the proteolytic cleavage of proIGF1R and proIR was obviously blocked in the cultured *Furin* knockout TECs (Figure 5C). In contrast, proIGF1R and proIR were normally processed into mature IGF1R and IR in cultured WT TECs (Figure 5C). The binding of IGF1R and IR to their ligands results in the autophosphorylation of the β subunit of IGF1R and IR (Hakuno and Takahashi, 2018). Consistently, the autophosphorylation of IGF1R and IR was obviously reduced in cultured *Furin* knockout TECs (Figure 5D). Next, we examined the alteration of the downstream signaling pathways of IGF1R and IR and observed a strong reduction in ERK phosphorylation in *Furin* knockout TECs compared with WT TECs (Figure 5D), indicating the downregulation of the ERK/MAPK signaling pathway in *Furin* knockout TECs. Moreover, the phosphorylation of Akt at either Thr308 or Ser473 also substantially decreased in *Furin* knockout TECs compared with WT TECs, which indicated the downregulation of the Akt signaling pathway in *Furin* knockout TECs (Figure 5D).

To directly prove the processing blockage of proIGF1R and proIR caused by *Furin* deletion *in vivo*, we sorted mTECs from 2-week-old WT and *Furin*$^{fl/fl}$*Foxn1*^{Cre} mice and examined the cleavage of proIGF1R and proIR by Simple Western. Coincident with the results obtained from the *in vitro* cultured TECs, we found that the cleavage of proIGF1R and proIR was also markedly blocked in mTECs of *Furin*$^{fl/fl}$*Foxn1*^{Cre} mice compared with WT mice (Figure 5E). To directly assess the effect of the processing blockage of proIGF1R and proIR on the downstream signaling pathway, we stimulated cultured WT and *Furin* knockout TECs using IGF1 and insulin, respectively. As expected, the addition of exogenous IGF1 or insulin promoted the autophosphorylation of IGF1R and IR and enhanced the downstream phosphorylation of ERK and Akt in WT TECs (Figure 5F). In contrast, *Furin* knockout TECs exhibited reduced phosphorylation of IGF1R and IR, as well as diminished phosphorylation of ERK and Akt, compared to WT TECs (Figure 5F). To further confirm the role of the ERK/MAPK and Akt signaling pathways in TEC development, we treated mice or FTOCs with ERK inhibitor (ERKi) and Akt inhibitor (AKTi), respectively. The results showed that administration of ERKi decreased the numbers of both mTECs and cTECs (Figure 5G) and that administration of AKTi significantly reduced the number of mTECs and had less effect on the number of cTECs (Figure 5H). Collectively, these results demonstrated that *Furin* ablation impaired the proteolytic cleavage of proIGF1R and proIR, which subsequently led to the downregulation of the ERK/MAPK and Akt signaling pathways.

Furin expression in thymic epithelial cells was indispensable for multiple stages of thymopoiesis

Next, we examined whether the impaired TEC microenvironment affected the development of thymocytes in 2-week-old *Furin*$^{fl/+}$*Foxn1*^{Cre} and *Furin*$^{fl/fl}$*Foxn1*^{Cre} mice. The frequency of early thymic precursors (ETPs), a population that is homing to thymus in response to chemokines CXCL12 and CCL25 expressed by cTECs (Abramson and Anderson, 2017; Liang et al., 2021; Zuklys et al., 2016), significantly decreased in *Furin*$^{fl/+}$-*Foxn1*^{Cre} and *Furin*$^{fl/fl}$*Foxn1*^{Cre} mice relative to littermate controls (Figure 6A). The subsequent progression of DN1 through DN4 was overtly similar among these mice, except for an obvious diminution of the DN1 subset in *Furin*$^{fl/+}$*Foxn1*^{Cre} and *Furin*$^{fl/fl}$*Foxn1*^{Cre} mice compared with WT mice (Figures S8A and S8B). The frequency of CD4 single-positive (CD4SP) and CD8 single-positive (CD8SP) thymocytes significantly decreased in 2-week-old *Furin*$^{fl/+}$*Foxn1*^{Cre} and *Furin*$^{fl/fl}$*Foxn1*^{Cre} mice compared with age-matched WT mice (Figure 6B), and the frequency of CD4^{+}CD8^{+} double-positive (DP) thymocytes was mildly increased (Figure 6B). The reduction of the CD4SP and CD8SP compartments correlated with impaired positive selection in *Furin*$^{fl/+}$*Foxn1*^{Cre} and *Furin*$^{fl/fl}$*Foxn1*^{Cre} mice, as the frequency of CD69^{+}TCRβ$^{int/hi}$ thymocytes markedly decreased compared with controls (Figure 6C). We next evaluated the cortical and medullary negative selection by assessing the frequency of DP and CD4SP thymocytes that co-expressed Helios and PD-1, respectively (Daley et al., 2013; Rodrigues et al., 2017). The negative selection of DP thymocytes, as defined by the co-expression of Helios and PD-1 on CD25^{-}DP thymocytes (Daley et al., 2013; Rodrigues et al., 2017), did not obviously change in *Furin*$^{fl/+}$*Foxn1*^{Cre} and *Furin*$^{fl/fl}$*Foxn1*^{Cre} mice in comparison with WT mice (Figures S8C and S8D). However, the negative selection of CD4SP thymocytes, as characterized by the

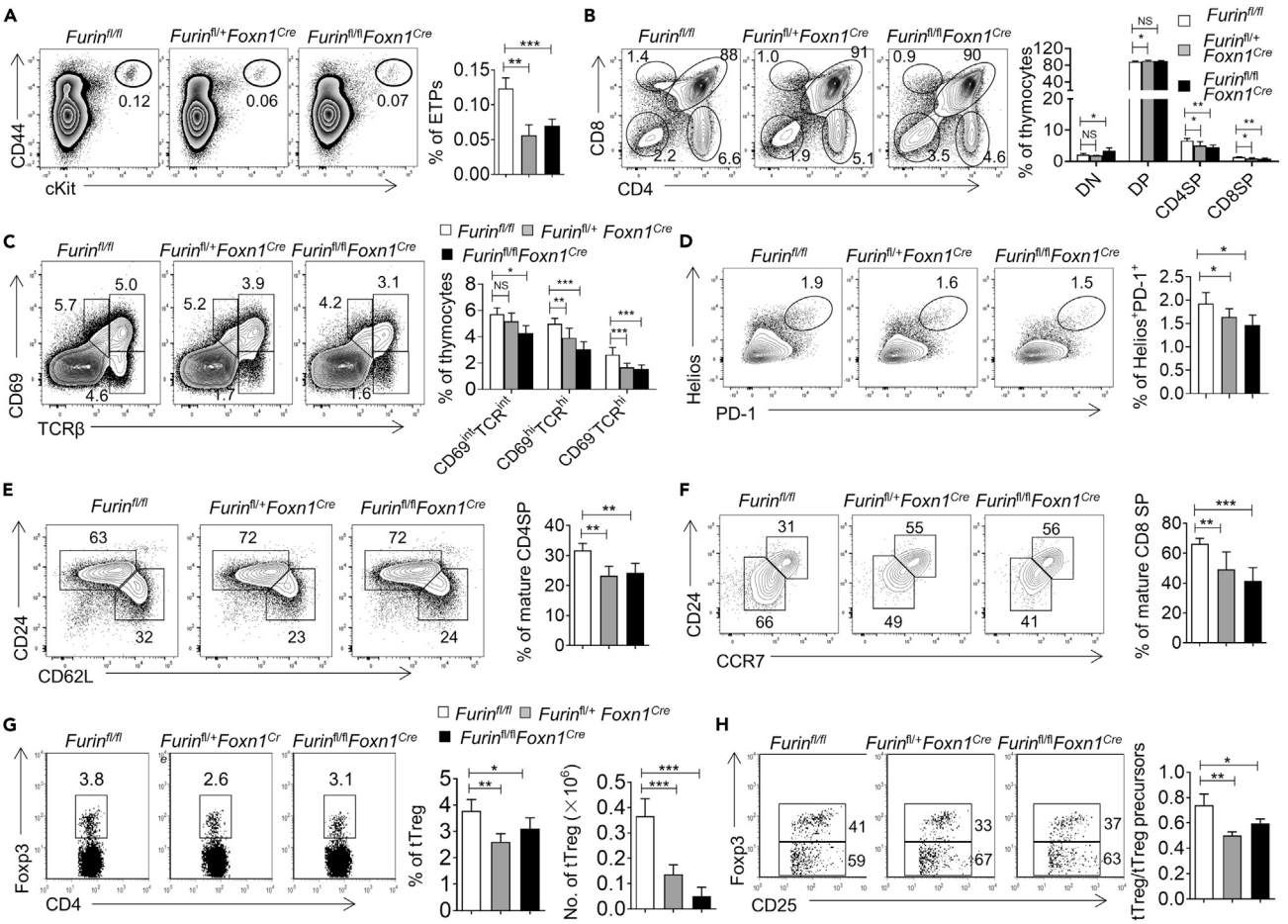

Figure 6. The development of thymocytes was disrupted in *Furin*$^{fl/+}$*Foxn1*^{Cre} and *Furin*$^{fl/fl}$*Foxn1*^{Cre} mice

(A) Flow cytometry plots for the expression of CD44 and cKit on CD25$^-$ thymocytes (left). Frequency of ETPs (CD44$^+$cKit$^+$CD25$^-$ thymocytes) (right). At least three mice were analyzed for each genotype.

(B) The distribution of DN, DP, CD4SP, and CD8SP populations among total thymocytes of 2-week-old WT (n = 6), *Furin*$^{fl/+}$*Foxn1*^{Cre} (n = 4), and *Furin*$^{fl/fl}$*Foxn1*^{Cre} (n = 4) mice.

(C) Relative distribution of thymocyte subpopulations with respect to CD69 and TCRβ expression in 2-week-old WT (n = 9), *Furin*$^{fl/+}$*Foxn1*^{Cre} (n = 7), and *Furin*$^{fl/fl}$*Foxn1*^{Cre} (n = 8) mice.

(D) The expression of Helios and PD-1 on TCRβ$^+$CD25$^-$CD4SP thymocytes of 2-week-old WT (n = 6), *Furin*$^{fl/+}$*Foxn1*^{Cre} (n = 5), and *Furin*$^{fl/fl}$*Foxn1*^{Cre} (n = 4) mice.

(E) The expression of CD24 and CD62L on TCRβ^{hi}CD4$^+$CD8$^-$ thymocytes.

(F) The expression of CD24 and CCR7 on TCRβ^{hi}CD5$^+$CD4$^-$CD8$^+$ thymocytes.

(G) Flow cytometric analysis and number of tTreg cells for each indicated genotype. tTreg cells are defined as CD4$^+$CD8$^-$Foxp3$^+$ thymocytes.

(H) Flow cytometric analysis for the expression of Foxp3 on CD4$^+$CD8$^-$CD25$^+$ thymocytes (left). The ratio showed the proportions of mature tTreg (CD4$^+$CD8$^-$CD25$^+$Foxp3$^+$) to the proportions of tTreg precursors (CD4$^+$CD8$^-$CD25$^+$Foxp3$^-$) for each genotype.

In panels (E–H), a minimum of three mice were analyzed per genotype. Data are represented as mean ± SD *p < 0.05; **p < 0.01; ***p < 0.001; NS, not statistically different.

co-expression of Helios and PD-1 on TCRβ$^+$CD25$^-$CD4SP thymocytes (Daley et al., 2013; Rodrigues et al., 2017), was significantly diminished in *Furin*$^{fl/+}$*Foxn1*^{Cre} and *Furin*$^{fl/fl}$*Foxn1*^{Cre} mice compared with WT control mice (Figure 6D). On the other hand, in addition to support the conventional αβ T cell development, TECs also promote the development of γ/δ T cells (Roberts et al., 2012). Our results showed that *Furin* ablation had no obvious effect on the proportion of αβ T cells and γ/δ T cells (Figures S8E and S8F).

The negatively selected thymocytes undergo further post-selection maturation in the medulla before they export as naive T cells to the periphery (Hauri-Hohl et al., 2014). The post-selection maturation of the thymocytes is marked by phenotypic and functional changes, including the upregulation of CD62L and the

downregulation of CD24 and CD69 (Eck et al., 2006; Li et al., 2007). The proportion of mature TCRβ^{hi}CD62L-^{hi}CD24^{lo} CD4SP thymocytes was significantly reduced in *Furin*$^{fl/+}$*Foxn1*^{Cre} and *Furin*$^{fl/fl}$*Foxn1*^{Cre} mice relative to WT control mice (Figure 6E), indicating a partial block in maturation. Similarly, CD8SP thymocytes in *Furin*$^{fl/+}$*Foxn1*^{Cre} and *Furin*$^{fl/fl}$*Foxn1*^{Cre} mice exhibited a decreased downregulation of CD24 (Figure 6F), suggesting an impaired maturation of these cells. It has been well known that mTECs also promoted the development of tTreg cells by agonist selection (Abramson and Anderson, 2017). The mature CD25$^+$Foxp3$^+$ tTreg cells in the thymus originate from CD25$^+$Foxp3$^-$ tTreg precursors (Josefowicz et al., 2012; Liang et al., 2018). The *Furin*$^{fl/+}$*Foxn1*^{Cre} and *Furin*$^{fl/fl}$*Foxn1*^{Cre} mice showed a reduced frequency and cell number of tTreg cells than WT controls (Figure 6G). We further showed that the reduction of tTreg cells in mutant mice was at least partially caused by the developmental blockage of CD25$^+$Foxp3$^-$ tTreg precursors into mature tTreg cells, as shown by the decreased ratio of CD25$^+$Foxp3$^+$ mature tTreg to CD25$^+$Foxp3$^-$ tTreg precursors (Figures 6H and S8G). More recent studies showed the existence of another mature tTreg development pathway in which mature CD25$^+$Foxp3$^+$ tTreg cells originate from immature CD25$^-$Foxp3$^+$ tTreg precursors (Cowan et al., 2016; Savage et al., 2020). We further examined the expression of CD25 versus Foxp3 in CD4$^+$CD8$^-$ thymocytes. The results showed that the percentage of immature CD25$^-$Foxp3$^+$ tTreg cells decreased in *Furin*$^{fl/+}$*Foxn1*^{Cre} and *Furin*$^{fl/fl}$*Foxn1*^{Cre} mice compared with WT mice (Figures S8H and S8I), indicating *Furin* ablation in TECs impaired the development of immature CD25$^-$Foxp3$^+$ tTreg cells. Collectively, these results indicated that homozygous or heterozygous deletion of *Furin* in TECs impaired TEC function in supporting thymocyte development marked by diminished ETPs, reduced positive and negative selection, partial blockage of post-selection maturation, and impaired tTreg generation.

Thymic tuft cells are critical for the development of type 2 invariant natural killer T (NKT2) cells, which further promote the generation of CD8$^+$EOMES$^+$SP thymocytes (Lee et al., 2013; Miller et al., 2018). Given the dramatic reduction of thymic tuft cells in *Furin*$^{fl/+}$*Foxn1*^{Cre} and *Furin*$^{fl/fl}$*Foxn1*^{Cre} mice, we detected the development of NKT2 and CD8$^+$EOMES$^+$SP thymocytes in these mice. The frequency and numbers of invariant natural killer T (iNKT) cells significantly decreased in *Furin*$^{fl/+}$*Foxn1*^{Cre} and *Furin*$^{fl/fl}$*Foxn1*^{Cre} mice compared with WT controls (Figures S9A and S9B). More importantly, the percentage and cellularity of NKT2 cells were drastically reduced in *Furin*$^{fl/+}$*Foxn1*^{Cre} and *Furin*$^{fl/fl}$*Foxn1*^{Cre} mice compared with littermate controls (Figures S9C–S9E). In contrast, the development of NKT1 and NKT17 cells was disturbed only in a much more moderate degree in *Furin*$^{fl/+}$*Foxn1*^{Cre} and *Furin*$^{fl/fl}$*Foxn1*^{Cre} mice relative to WT mice (Figures S9C–S9E). Moreover, the percentage and cellularity of CD8$^+$EOMES$^+$SP thymocytes were obviously reduced in *Furin*$^{fl/+}$*Foxn1*^{Cre} and *Furin*$^{fl/fl}$*Foxn1*^{Cre} mice in comparison with WT mice (Figures S9F and S9G). These results indicated that the defect of thymic tuft cells in *Furin*$^{fl/+}$*Foxn1*^{Cre} and *Furin*$^{fl/fl}$*Foxn1*^{Cre} mice led to the impaired development of NKT2 cells.

These perturbations in thymopoiesis extended to the peripheral T cell compartment in 4-week-old *Furin*$^{fl/+}$-*Foxn1*^{Cre} and *Furin*$^{fl/fl}$*Foxn1*^{Cre} mice, as indicated by diminished CD4 and CD8 T cell counts in spleen (Figure S10A). Importantly, the percentage and number of recent thymic emigrants (RTEs, which are defined as CD3$^+$CD4$^+$CD62L$^+$CD45RB^{int}) (Bredenkamp et al., 2014) were significantly diminished in *Furin*$^{fl/+}$*Foxn1*^{Cre} and *Furin*$^{fl/fl}$*Foxn1*^{Cre} mice in comparison with WT mice (Figure S10B). The CD4 and CD8 T cells in the spleen of *Furin*$^{fl/+}$*Foxn1*^{Cre} and *Furin*$^{fl/fl}$*Foxn1*^{Cre} mice displayed decreased CD62L$^+$CD44$^-$ naive phenotype and increased CD44$^+$CD62L$^+$ central memory and CD44$^+$CD62L$^-$ effector memory phenotype (Figure S11A). Although the percentage of Treg cells slightly increased, the number of Treg cells was drastically decreased in the spleen of 4-week-old *Furin*$^{fl/+}$*Foxn1*^{Cre} and *Furin*$^{fl/fl}$*Foxn1*^{Cre} mice in comparison with age-matched WT mice (Figure S11B). These results demonstrated that the homeostasis of peripheral T cells is disturbed in *Furin*$^{fl/+}$*Foxn1*^{Cre} and *Furin*$^{fl/fl}$*Foxn1*^{Cre} mice.

Thymic epithelial cell-expressed *Furin* was essential for the establishment of central immune tolerance

Mature mTECs express a wide spectrum of TRAs and present them directly, or indirectly through DCs, to developing thymocytes to impose T cell tolerance by eliminating self-reactive thymocytes from the αβTCR repertoire (Abramson and Anderson, 2017). A failure in this process leads to devastating autoimmunity. The impaired mTEC development in *Furin*$^{fl/+}$*Foxn1*^{Cre} and *Furin*$^{fl/fl}$*Foxn1*^{Cre} mice prompted us to detect the establishment of central immune tolerance in these mice. We evaluated the expression of AIRE-dependent and AIRE-independent TRAs (Table S4) in mTECs of WT, *Furin*$^{fl/+}$*Foxn1*^{Cre}, and *Furin*$^{fl/fl}$*Foxn1*^{Cre} mice using the RNA-seq data. The results showed that the expression of a large proportion of AIRE-dependent

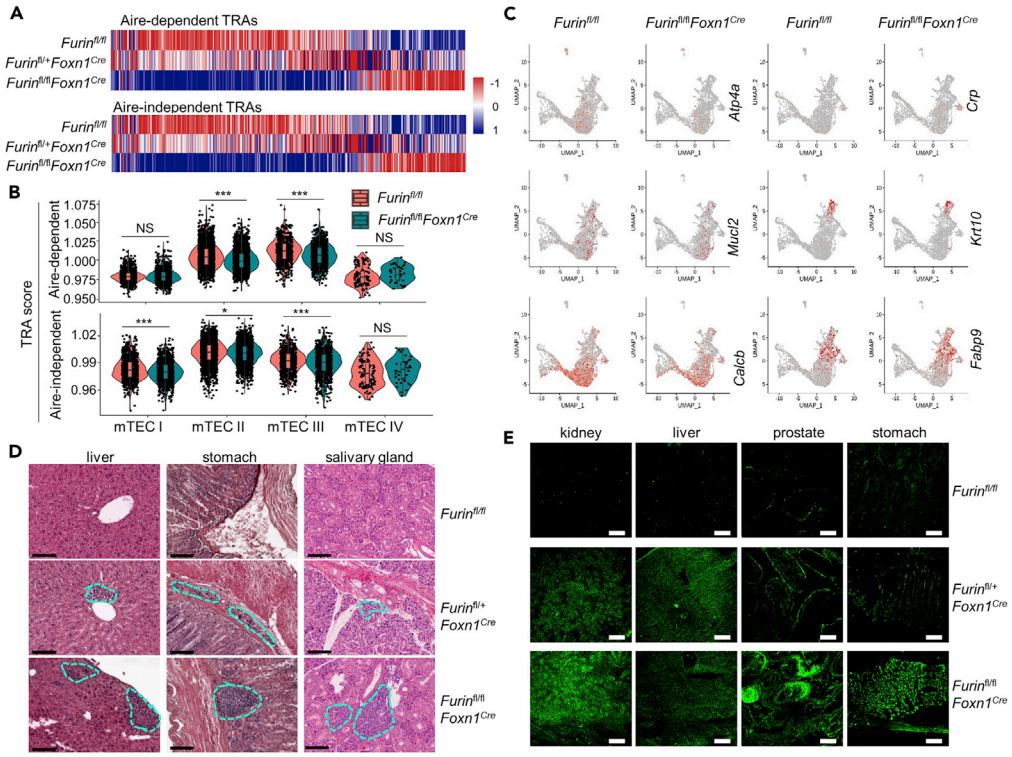

Figure 7. *Furin*$^{fl/+}$*Foxn1*^{Cre} and *Furin*$^{fl/fl}$*Foxn1*^{Cre} mice developed severe autoimmune disease

(A) Heatmap for the expression of AIRE-dependent and AIRE-independent TRAs in mTECs of 2-week-old WT, *Furin*$^{fl/+}$*Foxn1*^{Cre}, and *Furin*$^{fl/fl}$*Foxn1*^{Cre} mice according to bulk RNA-seq data.

(B) Violin plots of the AIRE-dependent and AIRE-independent TRA scores applied to cells at each indicated cell cluster according to the scRNA-seq data.

(C) UMAP plots showing the expression of representative TRAs in WT and *Furin*-deficient mTECs.

(D) Representative hematoxylin and eosin-stained histological sections of liver, stomach, and salivary gland from 6- to 8-month-old WT, *Furin*$^{fl/+}$*Foxn1*^{Cre}, and *Furin*$^{fl/fl}$*Foxn1*^{Cre} mice. Scale bars: 100 μm.

(E) Tissue-reactive autoantibodies in the sera of 6- to 8-month-old WT, *Furin*$^{fl/+}$*Foxn1*^{Cre}, and *Furin*$^{fl/fl}$*Foxn1*^{Cre} mice were examined using indicated tissue sections of *Rag2*$^{-/-}$ mice. Scale bars: 1,000 μm.

Data are represented as mean ± SD *p < 0.05; ***p < 0.001; NS, not statistically different.

and AIRE-independent TRAs was substantially downregulated in mTECs of *Furin*$^{fl/fl}$*Foxn1*^{Cre} mice compared with WT mice (Figure 7A). Many of the AIRE-dependent and AIRE-independent TRAs also moderately decreased in mTECs of *Furin*$^{fl/+}$*Foxn1*^{Cre} mice relative to WT mice (Figure 7A). We further examined the TRA expression level in individual mTEC cells of WT and *Furin*$^{fl/fl}$*Foxn1*^{Cre} mice by constructing a TRA score according to previously published information (Cowan et al., 2019). The frequency of cells with a high AIRE-dependent TRA score significantly declined in the mTEC II and III subsets, and the frequency of cells with a high AIRE-independent TRA score was obviously reduced in the mTEC I, II, and III subsets (Figure 7B). The expression of some representative TRAs in WT and *Furin*-deficient mTECs was shown in the UMAP plots (Figure 7C). These results illustrated that homozygous or heterozygous deletion of *Furin* in TECs disturbed the expression of many AIRE-dependent and AIRE-independent TRAs, which implied that these mice might develop autoimmune diseases. Indeed, we observed obvious signs of autoimmunity in 6- to 8-month-old *Furin*$^{fl/+}$*Foxn1*^{Cre} and *Furin*$^{fl/fl}$*Foxn1*^{Cre} mice, including weight loss, hunched posture, and hair slip, whereas the age-matched control mice were healthy (Figures S12A and S12B). Consistently, the 6- to 8-month-old *Furin*$^{fl/+}$*Foxn1*^{Cre} and *Furin*$^{fl/fl}$*Foxn1*^{Cre} mice developed marked lymphocytic infiltrations in multiple organs, such as liver, stomach, and salivary gland (Figures 7D and S12C). Moreover, these mice also displayed profound tissue cell-reactive autoantibodies against kidney, liver, prostate, and stomach in serum (Figure 7E and Table 1). In contrast, the age-matched control mice exhibited minimal lymphocytic infiltrations in these organs and showed no detectable autoantibody production in serum (Figures 7D, 7E, and S12C). Noticeably, the signs of autoimmunity in *Furin*$^{fl/+}$*Foxn1*^{Cre} mice were ameliorated compared with those in *Furin*$^{fl/fl}$*Foxn1*^{Cre} mice, which is coincident with the milder TEC impairment and TRAs dysregulation in

Table 1. Penetrance of autoantibody production in 6- to 8-month-old WT, *Furin*$^{fl/+}$*Foxn1*^{Cre}, and *Furin*$^{fl/fl}$*Foxn1*^{Cre} mice

Tissue	WT	*Furin*$^{fl/+}$*Foxn1*^{Cre}	*Furin*$^{fl/fl}$*Foxn1*^{Cre}
Kidney	0/4	2/4	4/4
Liver	0/4	3/4	3/4
Prostate	0/3	2/3	3/3
Stomach	1/4	2/4	3/4

See Figure 7.

Furin$^{fl/+}$*Foxn1*^{Cre} mice than *Furin*$^{fl/fl}$*Foxn1*^{Cre} mice. These results demonstrated that homozygous or heterozygous deletion of *Furin* in TECs resulted in the breakdown of T cell central immune tolerance.

DISCUSSION

We herein identified the critical role of proprotein convertase furin in the development of TECs. Ablation of *Furin* in TECs caused severe thymic atrophy and significantly reduced the cell number of TECs, and the number of mTECs and thymic tuft cells was decreased more dramatically than the cell number of cTECs after *Furin* inactivation in TECs. Notably, haploinsufficiency of *Furin* in TECs also caused obvious thymic atrophy and substantial numeric decline of TECs but less than full deletion of *Furin*. Thus, furin controls TEC development in a dose-dependent manner. In addition, *Furin* deletion also impaired the development of TECs at the embryonic stage. It has been shown that mTECs derived from progenitor cells expressing cTEC traits, including CD205, β5t, and so on (Baik et al., 2013; Ohigashi et al., 2013; Ribeiro et al., 2013) and Cld3,4^{hi}SSEA-1^{+} TECs was identified as mTEC progenitors (Sekai et al., 2014). Our results showed that *Furin* deletion had no obvious effect on the proportion of CD205^{+} TECs and Cld3,4^{hi}SSEA-1^{+} TECs, indicating *Furin* deletion did not alter the early development process of TECs.

Our series of studies with bioinformatic, molecular, biochemical, and flow cytometry assays further showed that *Furin* deficiency predominately impaired cell proliferation but not cell death/survival of TECs. *Furin* inactivation reduced the cell proliferation of mTECs and cTECs, which is coincident with the pro-proliferation role of furin in β cells and some cell lines (Bassi et al., 2017; Brouwers et al., 2020). Although some studies demonstrated that *Furin* deficiency promoted cell apoptosis in some cancers (He et al., 2020a, 2020b), our results showed that *Furin* inactivation in TECs had no detectable effect on the apoptosis of mTECs and cTECs. This inconsistency may be a result of the difference in cell types and local microenvironments.

Furin deficiency in TECs resulted in severe processing blockage of proIGF1R and proIR to biofunctional counterparts. IGF1R has been shown to possess a high affinity for IGF1 and IGF2; IR has been shown to possess a high affinity for insulin and IGF2 (Hakuno and Takahashi, 2018; Kitamura et al., 2003). It has been shown that IGF1 or insulin administration could restore thymus atrophy in diabetic rats (Binz et al., 1990). IGF1 could promote the development and cell proliferation of TECs *in vivo* and *in vitro* (Chu et al., 2008; Timsit et al., 1992). Consistent with the defect of IGF1R and IR in *Furin*-deleted TECs, the activation of their intracellular downstream signal pathways was decreased. *Furin* deficiency led to attenuation of the ERK/MAPK and Akt signaling pathways in TECs as indicated by the decreased phosphorylation of ERK1/2 and Akt in *Furin*-deleted TECs in response to IGF1 and insulin. Inhibiting ERK and Akt activation decreased the cell number of TECs *in vivo* and in the FTOC system. Collectively, all these data indicated that deletion of *Furin* in TECs impaired the cleavage of proIGF1R and proIR to functionally competent receptors, which subsequently decreased the downstream ERK/MAPK and Akt signaling pathways to finally cause the defect of TEC development.

Thymic tuft cells represent a terminally differentiated mTEC subset that is characterized by the expression of the canonical taste transduction pathway (Bornstein et al., 2018; Miller et al., 2018). The scRNA-seq analysis revealed that *Furin* inactivation had no obvious effect on the proportion of mTEC I, II, and III subsets but specifically reduced the percentage of mTEC IV subpopulations (thymic tuft cells). In addition, when subdivided mTECs into TAC-TEC, *Ccl21a*-high, *Aire*-positive, Late-*Aire*, and Tuft subsets according to another recent publication (Wells et al., 2020), *Furin* ablation also only reduced the proportion of Tuft subsets. These data indicated that *Furin* deletion did not affect the early differentiation kinetics of mTECs but favorably blocked thymic tuft cell differentiation.

TECs are essential for the stepwise development and maturation of conventional αβ T cells and unconventional T cell lineages (Abramson and Anderson, 2017). *Furin* inactivation in TECs impaired multiple stages of thymopoiesis, including generation of ETPs, positive and negative selection of thymocytes, and development of nTreg cells. Although the numbers of cTECs only decreased slightly in mutant mice, some cTEC-dependent thymocyte development was also impaired obviously, which may be caused by the reduced expression of some genes that are critical for early thymopoiesis in *Furin*-deficient cTECs. Additionally, the development of NKT2 was also severely compromised, which is related to impaired thymic tuft cell differentiation. Moreover, the impaired thymopoiesis in $Furin^{fl/+}Foxn1^{Cre}$ and $Furin^{fl/fl}Foxn1^{Cre}$ mice obviously disturbed peripheral T cell homeostasis as shown by the overrepresentation of activated/memory T cells and the reduction in the number of naive T and Treg cells. The appropriate expression of TRAs in mTECs is pivotal for T cells to establish central immune tolerance and to protect mice from suffering autoimmune disorders (Abramson and Anderson, 2017). *Furin* ablation remarkably interfered with the expression of many TRAs in mTECs as detected by RNA-seq and scRNA-seq assays. The reduced TRAs expression, impaired thymocyte negative selection and decreased Treg cell numbers in $Furin^{fl/+}Foxn1^{Cre}$ and $Furin^{fl/fl}Foxn1^{Cre}$ mice collectively resulted in the development of autoimmune disease with obvious organ infiltration of lymphocytes and autoreactive antibody production. So *Furin* expression in TECs is essential for the establishment of central immune tolerance, at least in mice. It is reported that aberrant furin activity is associated with the progression of some cancers and the enzymatic activity of furin is exploited by many bacterial and viral pathogens, including the current global pandemic SARS-CoV-2 (Braun and Sauter, 2019; Peacock et al., 2021). Thus, inhibition of furin activity has been an attractive approach in the treatment of malignant and infectious diseases (Couture et al., 2015; Wu et al., 2020). Considering the critical role of furin in maintaining T cell central and peripheral immune tolerance as shown by other and our present studies (Pesu et al., 2008), the potential side effects of furin inhibitors on the immune system should be recognized and should cause our caution.

Limitations of the study

In this study, we uncovered the role of furin in the development of TECs and in the establishment of central immune tolerance. We also showed that *Furin* ablation caused the defective cleavage of proIGF1R and proIR, which subsequently led to the attenuation of the downstream ERK/MAPK and Akt signaling pathways by using the *in vitro* cultured TECs. However, owing to the scarcity of TECs, we could not get enough primary TECs to examine the changes in ERK/MAPK and Akt signaling pathways by Western blot. Although we found that *Furin* deletion favorably impaired thymic tuft cell differentiation, we haven't fully uncovered the underlying mechanism. We should investigate these issues by integrating scRNA-seq, single cells transcriptomic assays, and spatially resolved proteomic analyses in the future.

STAR★METHODS

Detailed methods are provided in the online version of this paper and include the following:

- KEY RESOURCES TABLE
- RESOURCE AVAILABILITY
  - Lead contact
  - Materials availability
  - Data and code availability
- EXPERIMENTAL MODEL AND SUBJECT DETAILS
  - Mice
  - *In vitro* culture of TECs
- METHOD DETAILS
  - Flow cytometry analysis
  - Immunofluorescence staining
  - Isolation of thymic stromal cells
  - BrdU labeling and staining
  - 5-Ethynyl-2′-deoxyuridine (EdU) assay
  - Establishment of *Furin* overexpression cell line
  - Quantitative PCR
  - Bulk RNA-seq sample preparation and analysis
  - Single-cell RNA sequencing and analysis
  - Western blot

- Protein expression analysis by Simple Western
- ERK inhibitor and Akt inhibitor treatment
- Detection of autoantibodies

- QUANTIFICATION AND STATISTICAL ANALYSIS

SUPPLEMENTAL INFORMATION

Supplemental information can be found online at https://doi.org/10.1016/j.isci.2022.105233.

ACKNOWLEDGMENTS

We thank Dr. John W. M. Creemers for his generous gift of *Furin*$^{fl/fl}$ mice. We thank Mrs. Qing Meng for her expert technical assistance in cell sorting. This work was supported by grants from the National Natural Science Foundation of China for General and Key Programs (31930041, Y.Z., 31800754, Z.L.), the National Key Research and Development Program of China (2017YFA0105002, 2017YFA0104401, and 2017YFA0104402, Y.Z.), the Knowledge Innovation Program of Chinese Academy of Sciences (XDA16030301, Y.Z.).

AUTHOR CONTRIBUTIONS

Conceptualization, Z.F.L.; Methodology, Z.F.L. and Q.Z.; Software, Z.Q.Z.; Investigation, Z.F.L., Q.Z., X.D., T.L. and X.F.Y.; Resources, J.W. M.C; Visualization, Q.Z.; Writing, Z.F.L.; Supervision, Y.Z. and B.J.Z.

DECLARATION OF INTERESTS

The authors declare no competing interests.

Received: May 12, 2022
Revised: August 29, 2022
Accepted: September 25, 2022
Published: October 21, 2022

REFERENCES

Abramson, J., and Anderson, G. (2017). Thymic epithelial cells. Annu. Rev. Immunol. *35*, 85–118. https://doi.org/10.1146/annurev-immunol-051116-052320.

Al Rifai, O., Chow, J., Lacombe, J., Julien, C., Faubert, D., Susan-Resiga, D., Essalmani, R., Creemers, J.W., Seidah, N.G., and Ferron, M. (2017). Proprotein convertase furin regulates osteocalcin and bone endocrine function. J. Clin. Invest. *127*, 4104–4117. https://doi.org/10.1172/JCI93437.

Anderson, G., and Takahama, Y. (2012). Thymic epithelial cells: working class heroes for T cell development and repertoire selection. Trends Immunol. *33*, 256–263. https://doi.org/10.1016/j.it.2012.03.005.

Baik, S., Jenkinson, E.J., Lane, P.J.L., Anderson, G., and Jenkinson, W.E. (2013). Generation of both cortical and Aire(+) medullary thymic epithelial compartments from CD205(+) progenitors. Eur. J. Immunol. *43*, 589–594. https://doi.org/10.1002/eji.201243209.

Barthlott, T., Handel, A.E., Teh, H.Y., Wirasinha, R.C., Hafen, K., Žuklys, S., Roch, B., Orkin, S.H., de Villartay, J.P., Daley, S.R., and Holländer, G.A. (2021). Indispensable epigenetic control of thymic epithelial cell development and function by polycomb repressive complex 2. Nat. Commun. *12*, 3933. https://doi.org/10.1038/s41467-021-24158-w.

Bassi, D.E., Zhang, J., Renner, C., and Klein-Szanto, A.J. (2017). Targeting proprotein convertases in furin-rich lung cancer cells results in decreased in vitro and in vivo growth. Mol. Carcinog. *56*, 1182–1188. https://doi.org/10.1002/mc.22550.

Bessonnard, S., Mesnard, D., and Constam, D.B. (2015). PC7 and the related proteases Furin and Pace4 regulate E-cadherin function during blastocyst formation. J. Cell Biol. *210*, 1185–1197. https://doi.org/10.1083/jcb.201503042.

Binz, K., Joller, P., Froesch, P., Binz, H., Zapf, J., and Froesch, E.R. (1990). Repopulation of the atrophied thymus in diabetic rats by insulin-like growth factor I. Proc. Natl. Acad. Sci. USA *87*, 3690–3694. https://doi.org/10.1073/pnas.87.10.3690.

Bornstein, C., Nevo, S., Giladi, A., Kadouri, N., Pouzolles, M., Gerbe, F., David, E., Machado, A., Chuprin, A., Tóth, B., et al. (2018). Single-cell mapping of the thymic stroma identifies IL-25-producing tuft epithelial cells. Nature *559*, 622–626. https://doi.org/10.1038/s41586-018-0346-1.

Braun, E., and Sauter, D. (2019). Furin-mediated protein processing in infectious diseases and cancer. Clin. Transl. Immunol. *8*, e1073. https://doi.org/10.1002/cti2.1073.

Bredenkamp, N., Nowell, C.S., and Blackburn, C.C. (2014). Regeneration of the aged thymus by a single transcription factor. Development *141*, 1627–1637. https://doi.org/10.1242/dev.103614.

Brouwers, B., Coppola, I., Vints, K., Dislich, B., Jouvet, N., Van Lommel, L., Segers, C., Gounko, N.V., Thorrez, L., Schuit, F., et al. (2020). Loss of furin in beta cells induces an mTORC1-ATF4 anabolic pathway that leads to beta cell dysfunction. Diabetes *70*, 492–503. https://doi.org/10.2337/db20-0474.

Butler, A., Hoffman, P., Smibert, P., Papalexi, E., and Satija, R. (2018). Integrating single-cell transcriptomic data across different conditions, technologies, and species. Nat. Biotechnol. *36*, 411–420. https://doi.org/10.1038/nbt.4096.

Chu, Y.W., Schmitz, S., Choudhury, B., Telford, W., Kapoor, V., Garfield, S., Howe, D., and Gress, R.E. (2008). Exogenous insulin-like growth factor 1 enhances thymopoiesis predominantly through thymic epithelial cell expansion. Blood *112*, 2836–2846. https://doi.org/10.1182/blood-2008-04-149435.

Couture, F., Kwiatkowska, A., Dory, Y.L., and Day, R. (2015). Therapeutic uses of furin and its inhibitors: a patent review. Expert Opin. Ther. Pat. *25*, 379–396. https://doi.org/10.1517/13543776.2014.1000303.

Cowan, J.E., Malin, J., Zhao, Y., Seedhom, M.O., Harly, C., Ohigashi, I., Kelly, M., Takahama, Y., Yewdell, J.W., Cam, M., and Bhandoola, A. (2019). Myc controls a distinct transcriptional program in fetal thymic epithelial cells that determines thymus growth. Nat. Commun. *10*, 5498. https://doi.org/10.1038/s41467-019-13465-y.

Cowan, J.E., McCarthy, N.I., and Anderson, G. (2016). CCR7 controls thymus recirculation, but not production and emigration, of Foxp3(+) T cells. Cell Rep. *14*, 1041–1048. https://doi.org/10.1016/j.celrep.2016.01.003.

Daley, S.R., Hu, D.Y., and Goodnow, C.C. (2013). Helios marks strongly autoreactive CD4+ T cells in two major waves of thymic deletion distinguished by induction of PD-1 or NF-kappaB. J. Exp. Med. *210*, 269–285. https://doi.org/10.1084/jem.20121458.

de Mello Coelho, V., Villa-Verde, D.M.S., Farias-de-Oliveira, D.A., de Brito, J.M., Dardenne, M., and Savino, W. (2002). Functional insulin-like growth factor-1/insulin-like growth factor-1 receptor-mediated circuit in human and murine thymic epithelial cells. Neuroendocrinology *75*, 139–150. https://doi.org/10.1159/000048230.

Eck, S.C., Zhu, P., Pepper, M., Bensinger, S.J., Freedman, B.D., and Laufer, T.M. (2006). Developmental alterations in thymocyte sensitivity are actively regulated by MHC class II expression in the thymic medulla. J. Immunol. *176*, 2229–2237. https://doi.org/10.4049/jimmunol.176.4.2229.

Hakuno, F., and Takahashi, S.I. (2018). IGF1 receptor signaling pathways. J. Mol. Endocrinol. *61*, T69–T86. https://doi.org/10.1530/JME-17-0311.

Hamazaki, Y., Fujita, H., Kobayashi, T., Choi, Y., Scott, H.S., Matsumoto, M., and Minato, N. (2007). Medullary thymic epithelial cells expressing Aire represent a unique lineage derived from cells expressing claudin. Nat. Immunol. *8*, 304–311. https://doi.org/10.1038/ni1438.

Hanzelmann, S., Castelo, R., and Guinney, J. (2013). GSVA: gene set variation analysis for microarray and RNA-seq data. BMC Bioinf. *14*, 7. https://doi.org/10.1186/1471-2105-14-7.

Hauri-Hohl, M., Zuklys, S., Holländer, G.A., and Ziegler, S.F. (2014). A regulatory role for TGF-beta signaling in the establishment and function of the thymic medulla. Nat. Immunol. *15*, 554–561. https://doi.org/10.1038/ni.2869.

He, Z., Khatib, A.M., and Creemers, J.W.M. (2020a). Loss of proprotein convertase furin in mammary gland impairs proIGF1R and proIR processing and suppresses tumorigenesis in triple negative breast cancer. Cancers *12*, E2686. https://doi.org/10.3390/cancers12092686.

He, Z., Thorrez, L., Siegfried, G., Meulemans, S., Evrard, S., Tejpar, S., Khatib, A.M., and Creemers, J.W.M. (2020b). The proprotein convertase furin is a pro-oncogenic driver in KRAS and BRAF driven colorectal cancer. Oncogene *39*, 3571–3587. https://doi.org/10.1038/s41388-020-1238-z.

Jaaks, P., and Bernasconi, M. (2017). The proprotein convertase furin in tumour progression. Int. J. Cancer *141*, 654–663. https://doi.org/10.1002/ijc.30714.

Josefowicz, S.Z., Lu, L.F., and Rudensky, A.Y. (2012). Regulatory T cells: mechanisms of differentiation and function. Annu. Rev. Immunol. *30*, 531–564. https://doi.org/10.1146/annurev.immunol.25.022106.141623.

Kadouri, N., Nevo, S., Goldfarb, Y., and Abramson, J. (2019). Thymic epithelial cell heterogeneity: TEC by TEC. Nat. Rev. Immunol. *20*, 239–253. https://doi.org/10.1038/s41577-019-0238-0.

Khatib, A.M., Siegfried, G., Prat, A., Luis, J., Chrétien, M., Metrakos, P., and Seidah, N.G. (2001). Inhibition of proprotein convertases is associated with loss of growth and tumorigenicity of HT-29 human colon carcinoma cells: importance of insulin-like growth factor-1 (IGF-1) receptor processing in IGF-1-mediated functions. J. Biol. Chem. *276*, 30686–30693. https://doi.org/10.1074/jbc.M101725200.

Kitamura, T., Kahn, C.R., and Accili, D. (2003). Insulin receptor knockout mice. Annu. Rev. Physiol. *65*, 313–332. https://doi.org/10.1146/annurev.physiol.65.092101.142540.

Lee, Y.J., Holzapfel, K.L., Zhu, J., Jameson, S.C., and Hogquist, K.A. (2013). Steady-state production of IL-4 modulates immunity in mouse strains and is determined by lineage diversity of iNKT cells. Nat. Immunol. *14*, 1146–1154. https://doi.org/10.1038/ni.2731.

Li, J., Li, Y., Yao, J.Y., Jin, R., Zhu, M.Z., Qian, X.P., Zhang, J., Fu, Y.X., Wu, L., Zhang, Y., and Chen, W.F. (2007). Developmental pathway of CD4+CD8- medullary thymocytes during mouse ontogeny and its defect in Aire-/- mice. Proc. Natl. Acad. Sci. USA *104*, 18175–18180. https://doi.org/10.1073/pnas.0708884104.

Liang, Z., Zhang, L., Su, H., Luan, R., Na, N., Sun, L., Zhao, Y., Zhang, X., Zhang, Q., Li, J., et al. (2018). MTOR signaling is essential for the development of thymic epithelial cells and the induction of central immune tolerance. Autophagy *14*, 505–517. https://doi.org/10.1080/15548627.2017.1376161.

Liang, Z., Zhang, Q., Zhang, Z., Sun, L., Dong, X., Li, T., Tan, L., Xie, X., Sun, L., and Zhao, Y. (2021). The development and survival of thymic epithelial cells require TSC1-dependent negative regulation of mTORC1 activity. J. Immunol. *207*, 2039–2050. https://doi.org/10.4049/jimmunol.2100463.

Love, M.I., Huber, W., and Anders, S. (2014). Moderated estimation of fold change and dispersion for RNA-seq data with DESeq2. Genome Biol. *15*, 550. https://doi.org/10.1186/s13059-014-0550-8.

Miller, C.N., Proekt, I., von Moltke, J., Wells, K.L., Rajpurkar, A.R., Wang, H., Rattay, K., Khan, I.S., Metzger, T.C., Pollack, J.L., et al. (2018). Thymic tuft cells promote an IL-4-enriched medulla and shape thymocyte development. Nature *559*, 627–631. https://doi.org/10.1038/s41586-018-0345-2.

Ohigashi, I., Zuklys, S., Sakata, M., Mayer, C.E., Zhanybekova, S., Murata, S., Tanaka, K., Holländer, G.A., and Takahama, Y. (2013). Aire-expressing thymic medullary epithelial cells originate from beta5t-expressing progenitor cells. Proc. Natl. Acad. Sci. USA *110*, 9885–9890. https://doi.org/10.1073/pnas.1301799110.

Peacock, T.P., Goldhill, D.H., Zhou, J., Baillon, L., Frise, R., Swann, O.C., Kugathasan, R., Penn, R., Brown, J.C., Sanchez-David, R.Y., et al. (2021). The furin cleavage site in the SARS-CoV-2 spike protein is required for transmission in ferrets. Nat. Microbiol. *6*, 899–909. https://doi.org/10.1038/s41564-021-00908-w.

Pesu, M., Watford, W.T., Wei, L., Xu, L., Fuss, I., Strober, W., Andersson, J., Shevach, E.M., Quezado, M., Bouladoux, N., et al. (2008). T-cell-expressed proprotein convertase furin is essential for maintenance of peripheral immune tolerance. Nature *455*, 246–250. https://doi.org/10.1038/nature07210.

Ribeiro, A.R., Rodrigues, P.M., Meireles, C., Di Santo, J.P., and Alves, N.L. (2013). Thymocyte selection regulates the homeostasis of IL-7-expressing thymic cortical epithelial cells in vivo. J. Immunol. *191*, 1200–1209. https://doi.org/10.4049/jimmunol.1203042.

Roberts, N.A., White, A.J., Jenkinson, W.E., Turchinovich, G., Nakamura, K., Withers, D.R., McConnell, F.M., Desanti, G.E., Benezech, C., Parnell, S.M., et al. (2012). Rank signaling links the development of invariant gammadelta T cell progenitors and Aire(+) medullary epithelium. Immunity *36*, 427–437. https://doi.org/10.1016/j.immuni.2012.01.016.

Rodrigues, P.M., Ribeiro, A.R., Perrod, C., Landry, J.J.M., Araújo, L., Pereira-Castro, I., Benes, V., Moreira, A., Xavier-Ferreira, H., Meireles, C., and Alves, N.L. (2017). Thymic epithelial cells require p53 to support their long-term function in thymopoiesis in mice. Blood *130*, 478–488. https://doi.org/10.1182/blood-2016-12-758961.

Roebroek, A.J.M., Taylor, N.A., Louagie, E., Pauli, I., Smeijers, L., Snellinx, A., Lauwers, A., Van de Ven, W.J.M., Hartmann, D., and Creemers, J.W.M. (2004). Limited redundancy of the proprotein convertase furin in mouse liver. J. Biol. Chem. *279*, 53442–53450. https://doi.org/10.1074/jbc.M407152200.

Roebroek, A.J., Umans, L., Pauli, I.G., Robertson, E.J., van Leuven, F., Van de Ven, W.J., and Constam, D.B. (1998). Failure of ventral closure and axial rotation in embryos lacking the proprotein convertase Furin. Development *125*, 4863–4876.

Sansom, S.N., Shikama-Dorn, N., Zhanybekova, S., Nusspaumer, G., Macaulay, I.C., Deadman, M.E., Heger, A., Ponting, C.P., and Holländer, G.A. (2014). Population and single-cell genomics reveal the Aire dependency, relief from Polycomb silencing, and distribution of self-antigen expression in thymic epithelia. Genome Res. *24*, 1918–1931. https://doi.org/10.1101/gr.171645.113.

Savage, P.A., Klawon, D.E.J., and Miller, C.H. (2020). Regulatory T cell development. Annu. Rev. Immunol. *38*, 421–453. https://doi.org/10.1146/annurev-immunol-100219-020937.

Seidah, N.G., and Prat, A. (2012). The biology and therapeutic targeting of the proprotein convertases. Nat. Rev. Drug Discov. *11*, 367–383. https://doi.org/10.1038/nrd3699.

Sekai, M., Hamazaki, Y., and Minato, N. (2014). Medullary thymic epithelial stem cells maintain a functional thymus to ensure lifelong central T cell tolerance. Immunity *41*, 753–761. https://doi.org/10.1016/j.immuni.2014.10.011.

Shakib, S., Desanti, G.E., Jenkinson, W.E., Parnell, S.M., Jenkinson, E.J., and Anderson, G. (2009). Checkpoints in the development of thymic

cortical epithelial cells. J. Immunol. *182*, 130–137. https://doi.org/10.4049/jimmunol.182.1.130.

Susan-Resiga, D., Essalmani, R., Hamelin, J., Asselin, M.C., Benjannet, S., Chamberland, A., Day, R., Szumska, D., Constam, D., Bhattacharya, S., et al. (2011). Furin is the major processing enzyme of the cardiac-specific growth factor bone morphogenetic protein 10. J. Biol. Chem. *286*, 22785–22794. https://doi.org/10.1074/jbc.M111.233577.

Takaba, H., Morishita, Y., Tomofuji, Y., Danks, L., Nitta, T., Komatsu, N., Kodama, T., and Takayanagi, H. (2015). Fezf2 orchestrates a thymic program of self-antigen expression for immune tolerance. Cell *163*, 975–987. https://doi.org/10.1016/j.cell.2015.10.013.

Thomas, G. (2002). Furin at the cutting edge: from protein traffic to embryogenesis and disease. Nat. Rev. Mol. Cell Biol. *3*, 753–766. https://doi.org/10.1038/nrm934.

Timsit, J., Savino, W., Safieh, B., Chanson, P., Gagnerault, M.C., Bach, J.F., and Dardenne, M. (1992). Growth-hormone and insulin-like growth factor-I stimulate hormonal function and proliferation of thymic epithelial-cells. J. Clin. Endocrinol. Metab. *75*, 183–188. https://doi.org/10.1210/jc.75.1.183.

Tirosh, I., Izar, B., Prakadan, S.M., Wadsworth, M.H., 2nd, Treacy, D., Trombetta, J.J., Rotem, A., Rodman, C., Lian, C., Murphy, G., et al. (2016). Dissecting the multicellular ecosystem of metastatic melanoma by single-cell RNA-seq. Science *352*, 189–196. https://doi.org/10.1126/science.aad0501.

Wells, K.L., Miller, C.N., Gschwind, A.R., Wei, W., Phipps, J.D., Anderson, M.S., and Steinmetz, L.M. (2020). Combined transient ablation and single-cell RNA-sequencing reveals the development of medullary thymic epithelial cells. Elife *9*, e60188. https://doi.org/10.7554/eLife.60188.

Wickham, H. (2016). Package 'ggplot2': Elegant Graphics for Data Analysis (Springer-Verlag New York).

Wu, C., Zheng, M., Yang, Y., Gu, X., Yang, K., Li, M., Liu, Y., Zhang, Q., Zhang, P., Wang, Y., et al. (2020). Furin, a potential therapeutic target for COVID-19. iScience, 101642. https://doi.org/10.1016/j.isci.2020.101642.

Zhao, Y., Shen, X., Na, N., Chu, Z., Su, H., Chao, S., Shi, L., Xu, Y., Zhang, L., and Shi, B. (2018). mTOR masters monocyte development in bone marrow by decreasing the inhibition of STAT5 on IRF8. Blood *131*, 1587–1599.

Zheng, G.X.Y., Terry, J.M., Belgrader, P., Ryvkin, P., Bent, Z.W., Wilson, R., Ziraldo, S.B., Wheeler, T.D., McDermott, G.P., Zhu, J., et al. (2017). Massively parallel digital transcriptional profiling of single cells. Nat. Commun. *8*, 14049. https://doi.org/10.1038/ncomms14049.

Zuklys, S., Handel, A., Zhanybekova, S., Govani, F., Keller, M., Maio, S., Mayer, C.E., Teh, H.Y., Hafen, K., Gallone, G., et al. (2016). Foxn1 regulates key target genes essential for T cell development in postnatal thymic epithelial cells. Nat. Immunol. *17*, 1206–1215. https://doi.org/10.1038/ni.3537.

STAR★METHODS

KEY RESOURCES TABLE

REAGENT or RESOURCE	SOURCE	IDENTIFIER
Antibodies		
Anti-Helios-APC	Biolegend	Cat#137221; RID:AB_10662535
Anti-Ki-67-PE	BD Biosciences	Cat#556027; RRID:AB_2266296
Anti-Foxp3-PE	Thermo Fisher Scientific	Cat#11-5773-82; RRID:AB_465243
Anti-RORγt-BV421	BD Biosciences	Cat#562894; RRID:AB_2687545
Anti-PLZF-AF488	Thermo Fisher Scientific	Cat#53-9320-80; RRID:AB_2574444
DCAMKL1 (DCLK1)	Abcam	Cat#ab31704; RRID:AB_873537
AF647-conjugated donkey anti-rabbit IgG (H+L)	Jackson ImmunoResearch Labs	Cat#711-605-152; RRID:AB_2492288
Anti-CD45-PerCP/Cy5.5	BioLegend	Cat#103132; RRID:AB_893340
Anti-EpCAM-PE/Cy7	BioLegend	Cat#118215; RRID:AB_1236477
Anti-Ly51-AF647	BioLegend	Cat#108312; RRID:AB_2099613
Anti-I-A/I-E-BV421	BioLegend	Cat#107632; RRID:AB_2650896
Anti-CD40-PE	BioLegend	Cat#124610; RRID:AB_1134075
Anti-CD4-FITC	BioLegend	Cat#100406; RRID:AB_312691
Anti-CD4-APC	BioLegend	Cat#100412; RRID:AB_312697
Anti-CD4-APC/Cy7	BioLegend	Cat#100414; RRID:AB_312699
Anti-CD8a-BV421	BioLegend	Cat#100738; RRID:AB_11204079
Anti-CD44-PE	BioLegend	Cat#103055; RRID:AB_2564043
Anti-TCRβ-PE/Cy7	BioLegend	Cat#109222; RRID:AB_893625
Anti-PD-1-PE/Cy7	BioLegend	Cat#135216; RRID:AB_10689635
Anti-CD5-APC	BioLegend	Cat#100625; RRID:AB_2563928
Anti-Ter119-FITC	BioLegend	Cat#116206; RRID:AB_313707
Anti-CCR7-PE	BioLegend	Cat#120106; RRID:AB_389358
Anti-CD80-PE	Thermo Fisher Scientific	Cat#12-0801-82; RRID:AB_465752
Anti-CD117-PE/Cy7	Thermo Fisher Scientific	Cat#25-1171-81; RRID:AB_469643
Anti-CD24-FITC	Thermo Fisher Scientific	Cat#11-0242-82; RRID:AB_464988
Anti-CD62L-PE	Thermo Fisher Scientific	Cat#12-0621-82; RRID:AB_465721
Anti-CD25-PE	Thermo Fisher Scientific	Cat#12-0251-82; RRID:AB_465607
Anti-CD45RB-FITC	Thermo Fisher Scientific	Cat#11-0455-82; RRID:AB_465064
Anti-CD11b-FITC	Thermo Fisher Scientific	Cat#11-0112-85; RRID:AB_464936
Anti-F4/80-FITC	Thermo Fisher Scientific	Cat#11-4801-82; RRID:AB_2637191
Anti-NK1.1-FITC	Thermo Fisher Scientific	Cat#11-5941-81; RRID:AB_465317
Anti-Ly51-BV786	BD Biosciences	Cat#740882; RRID:AB_2740531
Anti-TCRβ-FITC	BD Biosciences	Cat#553171; RRID:AB_394683
Anti-TCRγδ-FITC	BD Biosciences	Cat#553177; RRID:AB_394688
Fluorescein-labeled UEA1	Vector Laboratories	Cat#FL-1061; RRID:AB_2336767
CD1d tetramer	ProImmune	Cat#D001-2X
rabbit anti-K5	Covance	Cat#PRB-160P-100; RRID:AB_10063444
rat anti-K8	DSHB	Cat#TROMA-I; RRID:AB_531826
chicken anti-K5	Biolegend	Cat#905904; RRID:AB_2721743
anti-rabbit-HRP	KPL	Cat#070-1506
anti-mouse-HRP	KPL	Cat#074-1806

(*Continued on next page*)

Continued

REAGENT or RESOURCE	SOURCE	IDENTIFIER
β-Actin	Sigma-Aldrich	Cat#A5441; RRID:AB_476744
IGF-I receptor β	Cell Signaling Technology	Cat#9750; RRID:AB_10950969
Insulin receptor β	Cell Signaling Technology	Cat#23413
p-IGF1R/IR	Cell Signaling Technology	Cat#3024; RRID:AB_331253
ERK1/2	R and D Systems	Cat#AF1576; RRID:AB_354872
p-ERK1/2	R and D Systems	Cat#MAB1018; RRID:AB_2140122
AKT	R and D Systems	Cat#MAB2055; RRID:AB_2224581
p-AKT473	R and D Systems	Cat#MAB887; RRID:AB_10973140
p-AKT308	Cell Signaling Technology	Cat#4056; RRID:AB_331163
IGF1R antibody	Novus Biologicals	Cat#NBP1-77679; RRID:AB_11011902
Insulin receptor β	Cell Signaling Technology	Cat#3025
AF 488 AffiniPure donkey anti-rabbit IgG (H+L)	Jackson ImmunoResearch Labs	Cat#715-545-150; RRID:AB_2340846
Chemicals, peptides, and recombinant proteins		
Fixation/Permeabilization Concentrate	Thermo Fisher Scientific	Cat#00-5123-43
Fixation/Permeabilization Diluent	Thermo Fisher Scientific	Cat#00-5223-56
Cytofix/Cytoperm solution	BD Biosciences	Cat#554722
Perm/Wash the solution	BD Biosciences	Cat#554723
collagenase/dispase	Sigma-Aldrich	Cat#11097113001
DNAse I	Sigma-Aldrich	Cat#D5025
SYBR Premix Ex TaqTM	TaKaRa	Cat# RR420
CD45 MicroBeads	Miltenyi Biotec	Cat#130-052-301; RRID:AB_2877061
TRIzol reagent	Thermo Fisher	Cat#15596018
IGF1	Abcam	Cat#ab198569
Insulin	Beyotime	Cat#P3376-100IU
RIPA	Beyotime	Cat#P0013B
PMSF	Beyotime	Cat#ST506
PhosSTOP phosphatase inhibitor	Roche	Cat#04906845001
nonfat dried milk	OXOID	Cat#LP0031
SCH772984 (ERK inhibitor)	Selleck	Cat#S7101
MK-2206 2HCl (AKT inhibitor)	Selleck	Cat#S1078
PEG300	Selleck	Cat#S6704
Critical commercial assays		
PE Active Caspase-3 Apoptosis Kit	BD Biosciences	Cat#550914; RRID:AB_393957
APC BrdU Flow Kit	BD Biosciences	Cat#552598; RRID:AB_2861367
BeyoClick™ EdU Cell Proliferation Kit	Beyotime	Cat#C0078S
MicroElute Total RNA Kit	Omega Bio-tek	Cat# R683
SuperScript III Reverse Transcriptase Kit	Invitrogen	Cat#18080-093
Enhanced BCA Protein Assay Kit	Beyotime	Cat#P0010S
12-230 kDa Separation Module	ProteinSimple	SM-W002-1
Deposited data		
Bulk RNA-seq data	This paper	GEO: PRJNA794306
scRNA-seq data	This paper	GEO: GSE193456

(*Continued on next page*)

Continued

REAGENT or RESOURCE	SOURCE	IDENTIFIER
Experimental models: Cell lines		
1C6-mock	This paper	N/A
1C6-*Furin*	This paper	N/A
BOSC 23 cells	ATCC	Cat# CRL-11270
Experimental models: Organisms/strains		
Furin$^{loxp/loxp}$ mice	Roebroek et al., 2004	N/A
Foxn1-Cre mice	Liang et al., 2018	N/A
ER-Cre mice	Zhao et al., 2018	N/A
Oligonucleotides		
Furin-forward ATGCTCAAGGCCAGA AGATC	Roebroek et al., 2004	N/A
Furin-revere AATCTGTTCCCTGCTGA GGA	Roebroek et al., 2004	N/A
Foxn1-Cre-forward TGCCTAGACGTTGG TCCTCAT	Liang et al., 2018	N/A
Foxn1-Cre-revere AATGTTGCTGGATAGT TTTTACTGC	Liang et al., 2018	N/A
ER-Cre-primer1 TGTGGACAGAGGAGCCA TAAC	Zhao et al., 2018	N/A
ER-Cre-primer2 CATCACTCGTTGCA TCGACC	Zhao et al., 2018	N/A
ER-Cre-primer3 AAGACCCAACCAACAGCA	Zhao et al., 2018	N/A
Recombinant DNA		
Plasmid: MSCV-PGK-IRES-GFP empty vector	This paper	N/A
Plasmid: MSCV-PGK-Furin-IRES-GFP	This paper	N/A
Plasmid: pCL-Eco	Addgene	Cat# 12371; RRID:Addgene_12371
Software and algorithms		
GraphPad Prism Version 8.0	GraphPad	https://www.graphpad.com
FlowJo v10	FlowJo, LLC	https://www.flowjo.com/
Compass for SW	ProteinSimple	https://www.bio-techne.com/cn/brands/proteinsimple
cellranger-3.1.0	Zheng et al., 2017	https://support.10xgenomics.com/single-cell-gene-expression/software/overview/welcome
Seurat	Butler et al., 2018	https://satijalab.org/seurat/articles/install.html
ggplot2	Wickham, 2016	https://ggplot2.tidyverse.org/
deseq2	Love et al., 2014	https://bioconductor.org/packages/release/bioc/html/DESeq2.html

RESOURCE AVAILABILITY

Lead contact

Further information and requests for resources and reagents should be directed to and will be fulfilled by the lead contact, Yong Zhao (zhaoy@ioz.ac.cn).

Materials availability

Plasmids generated in this study are available upon request from the lead contact, Yong Zhao (zhaoy@ioz.ac.cn).

Data and code availability

The bulk RNA-seq data and scRNA-seq data for this study have been deposited at GEO and are publicly available as of the date of publication. Accession numbers are listed in the key resources table. All data reported in this paper will be shared by the lead contact upon request.

This study did not generate original code.

Any additional information required to reanalyze the data reported in this paper is available from the lead contact upon request.

EXPERIMENTAL MODEL AND SUBJECT DETAILS

Mice

All animal experiments were approved by the Animal Ethics Committee of the Institute of Zoology, Beijing, China. Male C57BL/6 mice (aged six weeks) were purchased from the Beijing Laboratory Animal Research Center (Beijing, China). TEC-conditional two-allele or one-allele *Furin* deletion mice (male and female) were generated by crossing *Furin*$^{loxp/loxp}$ mice (Roebroek et al., 2004) with *Foxn1*-Cre mice (Liang et al., 2018). Tamoxifen-induced *Furin* knockout mice (male and female) were obtained by crossing *Furin*$^{loxp/loxp}$ mice with ER-Cre mice (Zhao et al., 2018). *Furin*$^{loxp/loxp}$ mice were the generous gifts of Dr. John W. M. Creemers from the Department of Human Genetics, KU Leuven, Leuven, Belgium. All mice used in the study were bred under specific pathogen-free conditions.

In vitro culture of TECs

For *in vitro* TEC culture, thymi from ER-Cre-*Furin*$^{loxp/loxp}$ mice neonatal mice were digested as described below. Small thymic fragments from each step were collected and pooled. Fragments were allowed to settle and washed twice with CnT07 medium (CELLnTEC, CnT-BM.4). The remaining thymic explants were plated in 24-well plates with CnT07 medium and cultured at 37°C with 5% CO2 for 5 days.

METHOD DETAILS

Flow cytometry analysis

Single-cell suspensions were prepared and stained with anti-CD16/32 antibodies to block Fc receptors. For cell surface staining, single-cell suspensions were stained for 30 min at 4°C in FACS buffer (PBS containing 0.1% BSA, 0.02% NaN_3). For intracellular staining, cells were fixed and permeabilized with fixation buffer (eBioscience, 00-5123-43 and 00-5223-56) and permeabilization buffer or the Cytofix/Cytoperm (BD Biosciences, 554722) and Perm/Wash (BD Biosciences, 554723) solutions according to the manufacturer's instruction. The staining of CCR7 was performed at 37°C. Stained samples were acquired on LSRFortessa X-20 Cell Analyzer (BD Biosciences) or Gallios (Beckman Coulter) Flow Cytometer. The detailed information of the fluorochrome-conjugated antibodies used for flow cytometry were listed in key resources table.

Immunofluorescence staining

Tissues were embedded into optimum cutting temperature compounds. For the staining of K5 and K8, thymus was cut into 6 μm sections, and for the staining of DCLK1, the thymus tissue was cut into 25 μm sections. Sections were fixed with 4% paraformaldehyde and blocked with donkey serum, followed by overnight incubation with primary antibodies. After washing with PBS-0.05% Tween, sections were incubated with secondary antibodies for 1 hour at room temperature. Color images were made on the N-SIM Super-Resolution Confocal Microscope (Nikon, Tokyo, Japan). The following antibodies were used for staining: rabbit anti-K5 (Covance, clone AF138), rat anti-K8 (DSHB, Troma-I), chicken anti-K5 (Biolegend, 905904), and rabbit anti-DCAMKL1 (DCLK1) (Abcam, ab31704).

Isolation of thymic stromal cells

Mouse thymi were isolated, cleaned of fat, and cut into pieces with a dissection scissors. Tissue pieces were resuspended with DMEM containing 2% FBS, then moved into 15 mL tubes and pipetted up and down

several times. Fragments were allowed to settle before removing the medium and replacing it with 2 mL of digestion medium containing 1 mg/mL collagenase/dispase (Sigma-Aldrich, 11097113001) with 20 U/mL DNAse I (Sigma-Aldrich, D5025) in DMEM. Tubes were then incubated at 37°C for 45 min. At the end of the digestion, cell suspensions were gently agitated; then, 5 mL PBS containing 1% FBS and 5 mM EDTA were added to neutralize the digestion. Finally, the cells were centrifuged and resuspended in DMEM (containing 2% FBS), then counted.

BrdU labeling and staining

Two-week-old mice were intraperitoneally injected with BrdU (1 mg per mouse). Twenty-four hours later, the mice were sacrificed, and thymic stromal cells were prepared as described above. After cell surface staining, the BrdU staining was performed using the APC BrdU Flow Kit (BD Biosciences, 552598) according to the manufacturer's instructions.

5-Ethynyl-2′-deoxyuridine (EdU) assay

The mouse *Furin* cDNA was constructed into MSCV-PGK lentiviral vector. The mTEC cell line 1C6 was transfected with MSCV-PGK-*Furin* (1C6-*Furin*) or empty vector (1C6-mock), and stable transfected clones were selected and amplified. For the EdU assay, 1C6-mock and 1C6-*Furin* cell lines seeded in 12-well plates were cultured to 70% confluence and then treated with EdU (10 μM) for 2 hours. The EdU incorporation was detected using BeyoClick™ EdU Cell Proliferation Kit with Alexa Fluor 594 (Beyotime, C0078S) according to the manufacturer's instructions.

Establishment of *Furin* overexpression cell line

The full length of *Furin* cDNA was subcloned into retroviral vector MSCV-PGK followed by IRES and GFP (MSCV-PGK-Furin-IRES-GFP). For retrovirus production, 2.4 μg of MSCV-PGK-Furin-IRES-GFP or empty vector in combination with 0.3 μg of pCL-Eco retrovirus packaging vector was transfected into BOSC 23 cells using jetPRIME transfection reagent (Polyplus). The culture supernatant containing retrovirus was collected after 48 and 72 hours through 0.45-μm filters. 1C6 cells was transduced by retrovirus carrying MSCV-PGK-Furin-IRES-GPF (1C6-Furin) or empty vector (1C6-mock). The single transduced cells were sorted using a Fusion cell sorter according to the expression of GFP, the the sorted cells was amplified and passaged to establish stable cell line.

Quantitative PCR

Single-cell thymic stromal suspensions were isolated and stained with appropriate antibodies, and mTECs were then sorted using an FACS BD fusion (BD Biosciences). RNA was isolated using the MicroElute Total RNA Kit (Omega Bio-tek, R6831) and reverse transcribed using the SuperScript III Reverse Transcriptase Kit (Invitrogen, 18080-093). The resulting cDNA was used as templates for quantitative PCR with SYBR Premix Ex Taq^{TM} (TaKaRa, RR420) on a CFX96 apparatus (Bio-Rad Laboratories).

Bulk RNA-seq sample preparation and analysis

Single-cell epithelial suspensions were isolated and enriched using anti-mouse CD45 microbeads (Miltenyi Biotec, 130052301), and cTECs and mTECs were then sorted using a Fusion cell sorter (BD Biosciences). The total RNA of the sorted cTECs and mTECs was extracted using TRIzol reagent (Thermo Fisher, 15596018), and amplified cDNA was prepared using the Smart-Seq2 method according to the manufacturer's instructions. Amplified cDNA quality was assessed by the Agilent 2100 High Sensitivity DNA Assay Kit (Agilent Technologies), and cDNA library construction was prepared using the Bioruptor Sonication System and CWBIO Gel Extraction Kit. After the library construction, the insertion size was assessed by the Agilent Bioanalyzer 2100 system, and the accurate insertion size was quantified by the TaqMan fluorescence probe of the AB Step One Plus Real-time PCR system (library valid concentration >10 nM). The libraries were then sequenced by an Illumina Hiseq platform with a 150 bp paired end. The raw data were assessed by FastQC, and the adaptor sequence was filtered by Trimgalore. We used the mapping software HISAT2 to map the reads to the mm10 reference genome and StringTie, to construct transcripts independently for each cell. The differentially expressed genes (q-value <0.05, |logfc| >0) were identified using DEGseq by comparing mTECs and cTECs from *Furin*$^{fl/+}$*Foxn1*^{Cre} and *Furin*$^{fl/fl}$*Foxn1*^{Cre} mice to those in WT mice, respectively. The differentially expressed genes were subjected to GSVA to calculate individual gene set enrichment scores by searching the c2.all.v7.4.symbols database according to published methods (Cowan et al., 2019; Hanzelmann et al., 2013). Visualization of GSVA results was obtained using R3.6.0. We used the

DAVID Bioinformatics Resources 6.8 online search tool (https://david.ncifcrf.gov/) and the Kobas online search tool (http://kobas.cbi.pku.edu.cn/) to search for gene ontology (GO) functional annotation and KEGG pathway analysis using all differential genes. All analyses were selected with $p < 0.05$ as the cutoff criterion. The bulk RNA sequencing data sets for this study can be found in Gene Expression Omnibus (GEO): PRJNA794306.

Single-cell RNA sequencing and analysis

The TECs from 2-week-old WT and *Furin*$^{fl/fl}$*Foxn1*^{Cre} mice were sorted using a Fusion cell sorter (BD Biosciences). Barcoded single cells were captured using the 10X Chromium microfluidics system (10X Genomics). Single-cell RNA-seq libraries were constructed using the Single Cell 3′ Library and Gel Bead Kit V3.1 (10X Genomics, 1000075) according to the manufacturer's instructions. Finally, the libraries were sequenced using an Illumina Novaseq 6000 sequencer with a sequencing depth of at least 100,000 reads per cell with pair-end 150 bp (PE150) reading strategy (performed by CapitalBio Technology, Beijing). The Cell Ranger pipeline (10X Genomics, version 3.0.2) was used to demultiplex cellular barcodes.

Sequences from scRNA-seq were processed using cellranger-3.0.2 software and the sequences were processed using the cellranger-mm10-3.0.0 genome and gtf file. Raw data generated by Cellranger were then read into the Seurat v3.2.3 R package with at least 200 genes per cell and at least 3 cells. Cells with <5% mitochondrial gene count and expressing 200–5,000 detected genes were retained for a total of 12,979 cells (5,431 for WT and 7,547 for *Furin*$^{fl/fl}$*Foxn1*^{Cre} mice). The remaining cells and genes were used for downstream analysis. The data were normalized by using 'LogNormalize' method and data scaled with 'scale.factor=10000' from Seurat. For each sample, variable genes were found by using 'FindVariableGenes' with the following options mean.function = ExpMean, dispersion.function = LogVMR, x.low.cutoff = 0.1, x.high.cutoff = 8, y.cutoff =1. Then we use IntegrateData to create an 'integrated' data assay. For the initial analysis the returned variable genes were used as the gene list given to the RunPCA function. Clusters were determined using the 'FindClusters' function with the following options reduction.type = 'pca', dims_use = 1:20, resolution = 1. Then remove T cells\endothelial cells\immune cells according to CD3e\CD34\CD45 to get TECs. Further TEC dimensionality reduction was performed by using RunUMAP using the options reduction.type = 'pca', dims_use = 1:20, resolution = 0.5. Markers of each cluster were found using the 'FindMarkers' command and highly similar clusters were merged. mTECs dimensionality reduction was performed by using RunUMAP using the options reduction.type = 'pca', dims_use = 1:20, resolution = 1 and also merged highly similar clusters and mTECs were clustered into four major populations, according to a previous report (Bornstein et al., 2018). Differential gene expression was performed by running FindMarkers on all pair-wise clusters (so that differentially expressed genes could be shared between clusters). The threshold of differentially expressed genes is logfc.threshold = 0.25, test.use = "wilcox", min.pct = 0.1. To account for the TRA heterogeneity in the mTEC subsets, we used the function "AddModuleScore" from Seurat (Tirosh et al., 2016) and the list of AIRE-dependent and AIRE-independent TRA-associated genes (Sansom et al., 2014) to calculate AIRE-dependent and AIRE-independent scores for each cell; this score was then regressed out. The scRNA-seq sets for this study can be found in GEO: GSE193456.

Western blot

Tamoxifen (0.125 μM) and vehicles were administrated to the *in vitro* cultured TECs for 2 days. When needed, cultured TECs were starved overnight and stimulated with 100 ng/mL IGF1 (Abcam, ab198569) and 200 ng/mL Insulin (Beyotime, P3376-100IU) for 20 min. The *in vitro* cultured TECs were lysed with radioimmunoprecipitation assay (RIPA) (Beyotime, P0013B) containing PMSF (Beyotime, ST506) and PhosSTOP phosphatase inhibitors (Roche, 04906845001). Protein concentration was determined using the Enhanced BCA Protein Assay Kit (Beyotime, P0010S). Proteins were separated by SDS-polyacrylamide gel electrophoresis (SDS-PAGE) and transferred onto PVDF membrane (Merck Millipore, IPFL00010). The PVDF membrane was blocked with 5% nonfat dried milk (OXOID, LP0031) for 1–2 hours, then incubated overnight with primary antibodies on a shaker at 4°C. After washing three times with PBST, the PVDF membrane was incubated with HPR-coupled secondary antibodies, and the concentration of proteins was detected through chemiluminescence (Merck Millipore, WBKLS0500). The detailed information of primary and secondary antibodies used for western blot were listed in key resources table.

Protein expression analysis by Simple Western

The sorted mTECs were lysed with RIPA as described above. Simple Western was performed using 12–230 kDa Separation Module (ProteinSimple, SM-W002-1) according to the manufacturer's instructions.

The results were analyzed using Compass for SW (ProteinSimple). The primary antibodies used for Simple Western are as follows: β-Actin (Sigma-Aldrich, A5441), IGF1R antibody (Novus Biologicals, NBP1-77679), and Insulin receptor β (CST, 3025).

ERK inhibitor and Akt inhibitor treatment

The ERK inhibitor, SCH772984 (Selleck, S7101), was dissolved in 5% DMSO+30% PEG300 (Selleck, S6704) +65% deionized water. Four-week-old C57BL/6 mice were treated intraperitoneally with either SCH772984 (25 mg/kg) or vehicle once a day for 7 days. The Akt inhibitor, MK-2206 2HCl (Selleck, S1078), was dissolved in DMSO. The thymic lobes of FTOC (Liang et al., 2018) were treated with either MK-2206 2HCl (1 μM) or vehicle for 4 days and then digested for the examination of mTECs and cTECs by flow cytometry.

Detection of autoantibodies

For the detection of autoantibodies, serum was collected from 6- to 8-month-old WT, *Furin*$^{fl/+}$*Foxn1*^{Cre}, and *Furin*$^{fl/fl}$*Foxn1*^{Cre} mice. Various tissue sections from *Rag2*$^{-/-}$ mice were then stained with the serum at 1:50 dilution, followed by incubation with AF488 donkey anti-rabbit IgG (H+L) (Jackson ImmunoResearch Laboratories, 715-545-150). Images were acquired with a laser scanning N-SIM Super-Resolution Confocal Microscope (Nikon, Tokyo, Japan).

QUANTIFICATION AND STATISTICAL ANALYSIS

All data are presented as the means ± SD. The Student's unpaired *t*-test for comparison of means was used to compare groups. A p-value of <0.05 was considered statistically significant.